https://doi.org/10.5194/egusphere-2026-5287
Preprint. Discussion started: 28 October 2026
© Author(s) 2026. CC BY 4.0 License.

Peatland hydrology in Noah-MP land surface model v5.0: parameterization and evaluation over the Congo peatlands

Arijit Chakraborty[1,2], Patrick Willems[1], Gabriëlle J. M. De Lannoy[2], David M. Mocko[3,4], Sujay V. Kumar[3], Cenlin He[5], Landry N. Nkaba[7], Bart Crezee[8], Raphael M. Tshimanga[7], Augusto Getirana[3,6], and Michel Bechtold[2]

[1]Department of Civil Engineering, Hydraulics and Geotechnics Section, KU Leuven, Leuven, Belgium
[2]Department of Earth and Environmental Sciences, KU Leuven, Leuven, Belgium
[3]Hydrological Sciences Laboratory, NASA Goddard Space Flight Center, Greenbelt, MD, USA
[4]Science Applications International Corporation, Greenbelt, Maryland, USA
[5]NSF National Center for Atmospheric Research, Boulder, CO, USA
[6]Science Systems and Applications, Inc., Lanham, MD, USA
[7]Regional School of Water (ERE) & Congo Basin Water Resources Research Center (CRREBaC), University of Kinshasa, Kinshasa, Democratic Republic of the Congo
[8]School of Geography, University of Leeds, Leeds, UK

Correspondence: Arijit Chakraborty (arijit.chakraborty@kuleuven.be)

Abstract.

Tropical peatlands are carbon-rich ecosystems primarily governed by water level dynamics, yet they remain inadequately represented in many land surface models (LSMs). The widely used Noah-Multiparameterization (Noah-MP) LSM lacks peatland-specific parameterizations. This study presents enhanced capabilities of Noah-MP LSM v5.0 by implementing peatland-specific modules for microtopography-based subgrid inundation, a water-level-dependent runoff formulation, and evapotranspiration stress functions governed by water-level dynamics, along with the peat soil properties, in a similar way as earlier implemented in the NASA Catchment LSM with peatland-specific modules (PEATCLSM). These options are applied selectively to peat grid cells within the NASA Land Information System (LIS) framework, retaining default model physics elsewhere. We evaluate the scheme over the Cuvette Centrale, the world's largest tropical peatland complex in the central Congo Basin, using in-situ water levels from 20 monitoring wells and terrestrial water storage anomalies (TWSA) from the Gravity Recovery And Climate Experiment (GRACE) and GRACE Follow-On (GRACE-FO) satellite missions. Four experiments with two different input precipitation sources (MERRA-2 and CHIRPS) are conducted to differentiate the impacts of the peatland module from the default model, using the earlier developed PEATCLSM forced by MERRA-2 as a benchmark. The peat module substantially improves water level estimates, with CHIRPS-forced simulations achieving the highest performance (max correlations up to $R \approx 0.92$–0.95 at Mai-Ndombe with recent water level records) and reduced RMSE and bias relative to both the default Noah-MP and PEATCLSM when evaluated with in-situ data. The new peatland parameterization shifts simulated water levels from unrealistically dry conditions (median = -1.75 to -1.41 m) to wetland dynamics (median = -0.12 to -0.01 m), replacing Hortonian runoff with saturation-controlled subsurface flow (median = 1.78 to 1.87 mm day^{-1}) and reducing evapotranspiration (for CHIRPS reduced from about 3.2 to 2.86 mm day^{-1}), mainly due to waterlogging stress. At the basin scale, agreement

https://doi.org/10.5194/egusphere-2026-5287
Preprint. Discussion started: 28 October 2026
© Author(s) 2026. CC BY 4.0 License.

with satellite-based TWSA is improved with the inclusion of a proxy river storage component, increasing correlations (R) by up to 11.7% and reducing RMSE by 6.4%. These results underscore the value of explicit representations of peatland hydrology in the Noah-MP LSM and provide a modular basis for future model coupling and data assimilation.

1 Introduction

Peatlands are one of the most carbon-dense terrestrial ecosystems, with a naturally accumulated layer of peat at the surface (Page et al., 1999; Dommain et al., 2010). This carbon-rich layer of peat can be several meters in depth, formed by the partial decomposition of organic matter over thousands of years under persistently waterlogged and anaerobic conditions (Dargie et al., 2017; Dommain et al., 2011; Swindles et al., 2018; Hawthorne et al., 2023). Although peatlands only cover approximately 3–4% of the Earth's land surface (Page et al., 2011; Xu et al., 2018), they store a disproportionately large share of the global carbon pool estimated between 400-600 Pg C (Joosten and Clarke, 2002; Frolking et al., 2011; Loisel et al., 2014), exceeding the total plant biomass of the world (Turetsky et al., 2015; Uhde et al., 2025).

Globally, peatlands are categorized into ombrotrophic bogs, sustained primarily by precipitation, and the minerotrophic fens, which receive water from both precipitation and surface-groundwater sources (Bechtold et al., 2019). Most of these peatlands are located in boreal and temperate zones (Page et al., 2006, 2011; Waite, 1993). However, recent discoveries have underscored the global importance of tropical peatlands in Southeast Asia, Africa, the Caribbean, and Central and South America (Leifeld and Menichetti, 2018; Page et al., 2011; Dargie et al., 2017; Ribeiro et al., 2021). Tropical peatlands cover 13% of the global peatland area and store about 152-288 Pg C (Ribeiro et al., 2021; Page et al., 2011; Dargie et al., 2017). Their carbon density often surpasses that of other terrestrial ecosystems, including upland tropical forests and boreal peatlands (Honorio Coronado et al., 2021; Temmink et al., 2022), making them quite sensitive to climate change and anthropogenic influences (Biddulph et al., 2023; Dargie et al., 2017).

The improved understanding of peat-specific hydrological processes has facilitated the development of small-scale hydrological models designed for investigating the seasonal and interannual variability in water levels as well as contrasts between natural and drained tropical peatlands from fine-scale microtopography to regional-scale groundwater systems (Baird et al., 2017; Cobb et al., 2017; Mezbahuddin et al., 2015; Ishii et al., 2016; Wösten et al., 2008). Contemporary earth system models (ESMs) used for projecting future climate scenarios generally lack an explicit representation of peatland ecosystems (Loisel et al., 2021). Although the growing need to accurately quantify greenhouse gas emissions has driven the development of advanced biogeochemical modules reliant on a realistic representation of peatland hydrological processes, the parameterization of these processes remains challenging at large spatial scales (Limpens et al., 2008). One way to address this limitation is by incorporating peatland physics in land surface models (LSMs), which simulate land surface processes and the hydrological cycle to provide land energy and water fluxes to earth system models. Recent studies have increasingly focused on incorporating peat-specific hydrological processes into LSMs. These developments have been implemented across a range of models, including the Canadian Land Surface Scheme (CLASS; Wu et al., 2016) and its successor model, CLASS including biogeochemical cycles (CLASSIC v1.0; Melton et al., 2020), the Lund-Potsdam-Jena (LPJ) model (Wania et al., 2009), the Community Land

https://doi.org/10.5194/egusphere-2026-5287
Preprint. Discussion started: 28 October 2026
© Author(s) 2026. CC BY 4.0 License.

Model (CLM; Shi et al., 2015), the Organizing Carbon and Hydrology In Dynamic Ecosystems (ORCHIDEE; Qiu et al., 2018) LSM, and the Catchment Land Surface Model (CLSM) with its peatland modules (PEATCLSM; Bechtold et al., 2019). These models differ in how peatland hydrology was implemented. For example, the influence of peatland microtopography on the hydrology of peatlands is only represented in CLM and PEATCLSM, while most other models represent solely ombrotrophic conditions. In the peatland module of ORCHIDEE, surface runoff generated from the non-peatland portion of a grid cell is redirected as an additional water input to the peatland fraction representing the hydrological conditions of minerotrophic peatlands (fens). All the aforementioned peatland hydrological implementations focus on natural northern (mid to high latitude boreal and temperate) peatlands only.

Although tropical and northern peatlands share several common features, differences in their structure and physical characteristics result in contrasting hydrological dynamics. By adapting the northern peatland representation in PEATCLSM by Bechtold et al. (2019), Apers et al. (2022) developed the first, large-scale hydrological modules applicable for both natural and drained tropical peatlands. However, due to the lack of data from other tropical peatlands, the modules were parametrized based on literature data collected for Southeast Asian peatlands only. Consequently, the simulated water levels showed poor agreement with in-situ observations from the Cuvette Centrale (Apers et al., 2022).

In the version 7 of the NASA SMAP Level 4 Surface and Root Zone Soil Moisture (L4_SM) product (Reichle et al., 2023), SMAP Tb observations were assimilated into the PEATCLSM module globally over peatland-dominated grid cells. Later on, Apers et al. (2026) calibrated the soil hydraulic parameters and the discharge function for the Congo peatlands specifically through hydrological parameterization of in-situ water level dynamics using satellite-based precipitation based on the Rise-and-Recession analysis (Apers et al., 2025). Hence, currently, the PEATCLSM implementations only enable simulating the common hydrological processes separately for peat areas/pixels and provide separate diagnostic variables in this regard. However, the impact of water level fluctuations in the Congo River and its tributaries on the surrounding peatland hydrology remains unexplored and challenging to implement in the modeling scheme (Apers et al., 2026; Marthews et al., 2022; Biddulph et al., 2021). A combined hydrological-hydrodynamic coupled scheme can provide insights into the Cuvette Centrale hydrology more precisely.

The widely-used community Noah-Multiparameterization (Noah-MP; Niu et al., 2011; Yang et al., 2011; He et al., 2023b) model, serving as a key land component in various research and operational weather and hydrological models, includes multiple soil layers and a multi-layer snowpack, providing a more detailed vertical stratification than the three-variable prognostic approach of CLSM. The core advantage of Noah-MP is its ability to select from multiple physics options/parameterizations for the same process. Noah-MP v5.0 has been refactored (He et al., 2023b) into a highly modular structure, in which each physical process is a separate Fortran module. Furthermore, He et al. (2025) integrated this refactored version into the NASA Land Information System (LIS; Kumar et al., 2006, 2008; Peters-Lidard et al., 2007) and compared benchmark simulations from the new version against the previous iteration to assess global and regional performance. This makes it significantly easier for a developer to implement, read, and modify specific components like peatland hydrology in isolation without interfering with other parts of the code. Moreover, Noah-MP supports coupling with a river routing scheme, which will help to simulate the combined effect of peatland hydrology along with the river influence.

https://doi.org/10.5194/egusphere-2026-5287
Preprint. Discussion started: 28 October 2026
© Author(s) 2026. CC BY 4.0 License.

Considering these advantages, our study aims to incorporate peatland-specific hydrological functions into the Noah-MP LSM to establish a basis for future exploration of insights into peatland-river interactions in the Cuvette Centrale region. This paper describes the implementation of the PEATCLSM-like peatland physical functions into the refactored Noah-MP version 5.0, which enables model users to run peatland physical processes for identified peat grid cells, keeping other multi-physics options unchanged for non-peat pixels. The model capabilities have been enhanced to incorporate peatland hydrological processes by including peat soil hydraulic parameters, microtopographic integration, and new runoff and evapotranspiration schemes. This article is organized in the following manner: Section 2 provides an overview of the study area, including the peatland locations and monitoring well locations considered in this study. Section 3 describes the peatland-specific physical processes incorporated into Noah-MP. Section 4 gives the details of the experimental setup for the model simulations, including the meteorological forcings, model input parameters, and the design of the model experiments. Section 5 presents the evaluation datasets and metrics used to assess model performance. Section 6 presents the results, followed by discussions and conclusions in Sect. 7 and Sect. 8, respectively.

2 Study area

The Cuvette Centrale wetland complex, located in the center of the Congo Basin, is a low-gradient depression formed by alluvial deposits evolved in response to changes in climatic and environmental conditions throughout the late Quaternary period (Elenga et al., 1994; Dargie et al., 2017; Laraque et al., 2009; Garcin et al., 2022; Hawthorne et al., 2023; Menges et al., 2025), which favor long-term peat accumulation (Fig. 1). This region is nested within the Congo Basin, Africa's second-largest river basin, which has a total drainage area of approximately 3.7 million km^2 and covers over 12% of the African continent (Alsdorf et al., 2016). The Cuvette Centrale holds a significant share of the global carbon stock of tropical peat.

Congo peatlands experience bimodal precipitation due to the seasonal migration of the Intertropical Convergence Zone (ITCZ), but receive 35 to 40% less precipitation annually compared to the Amazon, making it particularly vulnerable to seasonal and long-term water deficits (Guan et al., 2015; Nicholson, 2022). Following the bimodal precipitation pattern, the region experiences two wet seasons, occurring in April–May and October–November, separated by short and generally mild dry periods. The mean annual temperature is 25.6°C with little variation throughout the year (Samba et al., 2008). The region receives high annual rainfall from 1600 mm yr^{-1} to 1800 mm yr^{-1} (Laraque et al., 1998; Samba et al., 2008), and supports extensive forested wetlands, ranging from palm-dominated to hardwood forests (Dargie et al., 2017). Beneath these inundated swamp forests, the Cuvette Centrale hosts the world's largest expanse of intact tropical peatlands (Dargie et al., 2017, 2019; Crezee et al., 2022). These peatlands cover an estimated area of 16.8 Mha spanning the Democratic Republic of the Congo (DRC) and the Republic of the Congo (ROC), with a mean peat thickness of 1.7 m and total carbon storage of 29.0 Pg C (Dargie et al., 2017; Crezee et al., 2022; Hawthorne et al., 2023; Lawson et al., 2015; Hastie et al., 2024).

The Cuvette Centrale comprises diverse hydrological and geomorphic regimes, which are reflected in its peatland distribution and characteristics (Crezee et al., 2022; Dargie et al., 2017). Ombrotrophic peatlands are mainly located in the northern region, especially in the Republic of the Congo, where interfluvial basins are likely flooded seasonally by rainfall rather than rivers

https://doi.org/10.5194/egusphere-2026-5287
Preprint. Discussion started: 28 October 2026
© Author(s) 2026. CC BY 4.0 License.

(Alsdorf et al., 2016; Datok et al., 2022). These areas are characterized by shallow peat domes, low flood depths (<0.6 m), and precipitation-driven hydrology (Lee et al., 2015; Davenport et al., 2020). These peat deposits typically have high organic carbon content (>50%) and thickness ranging from about 2 m to 6 m (Crezee et al., 2022).

In contrast, recent observations from the Democratic Republic of the Congo (DRC) have identified another favorable environment for peat development associated with river systems (Crezee et al., 2022). Peatlands in this region follow the dendritic pattern of the river network along some of the Congo's left-bank tributaries in DRC and next to the Congo main stream, and are expected to be influenced by river water due to high flooding in the main wet season (Lee et al., 2015). Despite these differences, peat deposits here have similar carbon concentrations and observed peat thickness as in the interfluvial basins (Crezee et al., 2022).

https://doi.org/10.5194/egusphere-2026-5287
Preprint. Discussion started: 28 October 2026
© Author(s) 2026. CC BY 4.0 License.

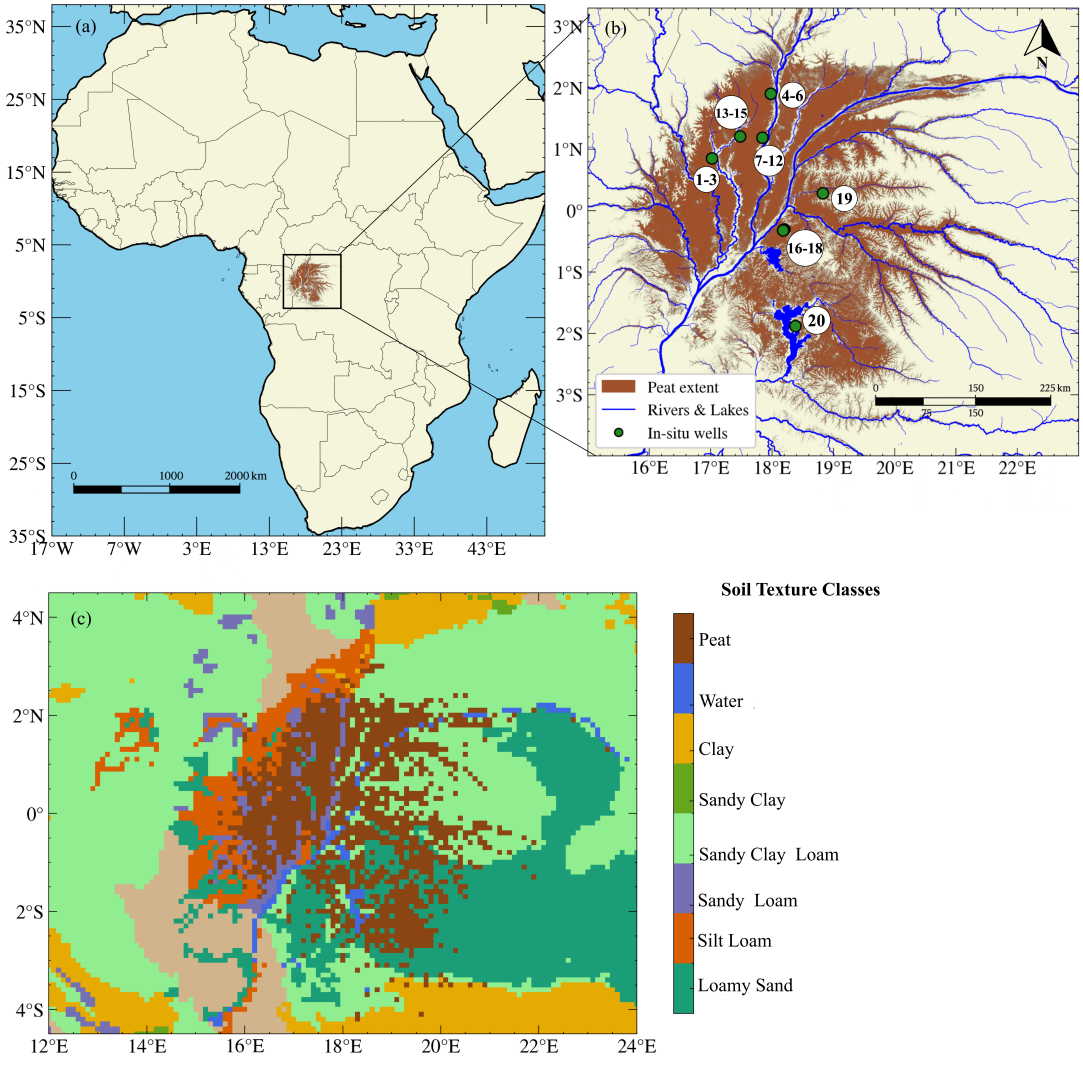


Figure 1. Study area: Cuvette Centrale peatlands located in Africa, shared by Republic of Congo and the Democratic Republic of Congo. The location of the monitoring wells in green with their serial number corresponding to the list of well locations in Table C1. Subplot (c) shows the soil texture classes as applied at the model resolution. Peatland distribution in (b) and (c) is based on Crezee et al. (2022)

3 Model description and peatland parameterization

3.1 Noah-Multiparameterization (Noah-MP)

The community Noah-Multiparameterization (Noah-MP; Niu et al., 2011; Yang et al., 2011) LSM was originally developed with an enhancement in the representation of land surface processes of the Noah LSM (Ek et al., 2003) by incorporating multiple physics options with various parameterizations and improved treatments of canopy-snow-soil-hydrology processes

https://doi.org/10.5194/egusphere-2026-5287
Preprint. Discussion started: 28 October 2026
© Author(s) 2026. CC BY 4.0 License.

and coupling (He et al., 2023a). For improved representation of soil moisture dynamics and handling the discretization process efficiently in its default configuration that is employed in this study, Noah-MP considers four soil layers with a total soil depth of 2 m. The thicknesses of the soil layers from the surface to the bottom are 0.1, 0.3, 0.6, and 1.0 m, respectively, with the root zone in the upper 1 m of soil.

Noah-MP allows multiple options for surface and subsurface runoff schemes of which two schemes that are available in the LIS allow the simulation of the groundwater level. Here, we use as a reference for the peatland-enabled model advancement the TOPMODEL-based groundwater and runoff scheme (Niu et al., 2007) which does not have a prognostic lateral flow or aquifer storage but infers groundwater from soil moisture assuming hydrostatic equilibrium. The alternative scheme with a prognostic aquifer storage is not designed for water table deeper than 1.5 m; this limit was systematically reached over the Cuvette Centrale, where the scheme consequently capped the simulated water level at a constant -1.5 m (from here onwards "water level" is the terminology used as negative of the water table depth variable of Noah-MP throughout the rest of the paper, allowing the sign convention to consider any water table rise above ground surface is positive and below ground surface as negative). In the TOPMODEL scheme, both surface and subsurface runoff are parameterized as exponential functions of the depth to the water table. The surface runoff [ms^{-1}] and infiltration rate [ms^{-1}] are computed as per Hortonian formulations when the total water input flux [ms^{-1}] into the top soil surface is greater than zero. Also, for soil hydraulics, Noah-MP has three different options. All these specific hydrological parameter options used in this study are listed in Table A1. More details on the latest Noah-MP v5.0 multi-physics options can be found on He et al. (2023a).

3.2 Peatland parameterizations implemented into Noah-MP

We implement in Noah-MP v5.0 the peatland-specific hydrological processes of PEATCLSM (Apers et al., 2026), while leaving the default Noah-MP physics for vegetation and energy unchanged. The peatland modifications are confined to the soil-hydrology modules governing infiltration, runoff, evapotranspiration, and water-level dynamics, and rest on a clear separation of two processes: microtopography controls how the grid-cell water storage and the inundated fraction respond to the water level, while vertical water movement within the peat is solved as a one-dimensional, pressure-head-based flow problem in which microtopography plays no role for computational feasibility. A new module, `PeatlandPhysicsMod`, activates these processes on the grid cells classified as peat.

3.2.1 Microtopography and surface ponding

Peatlands are nearly flat at the macrotopographic scale. TOPMODEL-based runoff schemes can therefore reproduce broad-scale wetland extent which often overlaps with peatland complexes (Stocker et al., 2014), but they are poorly suited to short-term peatland hydrological response, because many peatlands have become hydrologically decoupled from the wider catchment through peat accumulation and the low hydraulic conductivity of deeper peat. A rain-fed, peatland-specific treatment of soil-water dynamics has been shown to outperform TOPMODEL in reproducing measured peatland water level time series at the typical operating spatial scale of LSMs (Bechtold et al., 2019). At the microtopographic scale, by contrast, even small elevation differences between hummocks and hollows strongly control the fraction of the surface that gets inundated as the water level

https://doi.org/10.5194/egusphere-2026-5287
Preprint. Discussion started: 28 October 2026
© Author(s) 2026. CC BY 4.0 License.

rises towards it. Following Dettmann and Bechtold (2016), we therefore partition the grid-cell storage response between a soil domain and a ponded-surface domain, while keeping the vertical soil-water flux one-dimensional and pressure-head based for computational feasibility.

The subgrid surface elevation z_s [m], relative to the mean grid-cell elevation, is described in terms of a Gaussian distribution,

$$z_s \sim \mathcal{N}(0, \sigma_{\text{elev}}^2), \qquad z_s \in [-z_{\text{trunc}}, z_{\text{trunc}}], \tag{1}$$

with standard deviation $\sigma_{\text{elev}} = 0.16$ m, taken from the extensive surface-elevation survey in tropical peatlands from Lampela et al. (2016) and used to parameterize PEATCLSM for the tropical peatlands (Apers et al., 2022) and specifically Congo peatlands as well (Apers et al., 2026). The distribution is truncated at $\pm z_{\text{trunc}}$, with $z_{\text{trunc}} = 1.0$ m representing the top of the hummocks, which removes a negligible tail probability and is included to bound the elevation distribution physically. Each realization of the subgrid surface elevation z_s can be thought of as defining a single vertical soil column — a hypothetical 1-D soil profile whose local surface sits at elevation z_s within the grid cell. The inundated (ponded) fraction is the cumulative fraction of the surface lying below the instantaneous water level z_{wl} [m],

$$F_{\text{ponded}} = F_s(z_{\text{wl}}), \tag{2}$$

where F_s [-] is the cumulative distribution function of z_s. Internally, the model stores the water table as a single positive-downward state variable consistent with default Noah-MP conventions; the water level zwl used throughout this paper (positive above, negative below the surface) is the sign-inverted quantity, computed locally wherever the microtopography and stress formulations require it. In PEATCLSM, this ponded fraction is prescribed as an empirical function of water level; here it is diagnosed directly from the microtopographic elevation distribution. The surface-ponding storage is the depression storage filled below the water level,

$$S_{\text{surf}}(z_{\text{wl}}) = \int_{-z_{\text{trunc}}}^{z_{\text{wl}}} F_s(z)\,\mathrm{d}z, \tag{3}$$

and the soil water storage is the hydrostatic moisture profile integrated over the soil-occupied fraction of the column at each elevation,

$$S_{\text{soil}}(z_{\text{wl}}) = \int_{-z_{\text{bot}}}^{z_{\text{trunc}}} [1 - F_s(z)]\,\theta(z - z_{\text{wl}})\,\mathrm{d}z, \tag{4}$$

where z_{bot} [m] is the depth of the modeled soil column and the weighting factor $[1 - F_s(z)]$ is the fraction of the grid cell whose surface lies above elevation z. Equation (4) is the column average of the hydrostatic soil-water profile over the subgrid

https://doi.org/10.5194/egusphere-2026-5287
Preprint. Discussion started: 28 October 2026
© Author(s) 2026. CC BY 4.0 License.

surface-elevation distribution: a column whose surface lies at elevation z_s contains soil only up to z_s, so at a given elevation z the soil-filled fraction of the grid cell is the fraction of columns whose surface exceeds z, namely $[1 - F_s(z)]$; weighting the equilibrium moisture $\theta(z - z_{\mathrm{wl}})$ by this fraction and integrating over the column is equivalent to averaging the per-column soil-water storage over the elevation distribution, and reproduces the soil water storage and soil water specific-yield expressions of Dettmann and Bechtold (2016). Note that $[1 - F_s(z)]$ depends only on the surface-elevation distribution, not on the water level. It is the geometric fraction of columns whose own local surface lies at or above z, and therefore have soil physically present at that elevation, irrespective of whether that soil is saturated. The wetness of that soil is captured separately by $\theta(z - z_{\mathrm{wl}})$. Ponded surface water is excluded from S_{soil} [-] by construction: for a flooded column (whose local surface z_s lies below z_{wl}), the water occupying the interval between z_s and z_{wl} is accounted for in the surface storage term S_{surf} [-] (Eq. 3), not in S_{soil}.

The upper limit z_{trunc} extends the integration above the mean surface ($z = 0$) into the hummocks, retaining the soil moisture held in those parts of the microtopography that rise above the mean elevation. The hydrostatic profile uses the Campbell retention relation (Campbell, 1974), inverted to give moisture as a function of suction ψ,

$$\theta(\psi) = \begin{cases} \theta_s, & \psi \le \psi_s, \\ \theta_s \left(\dfrac{\psi}{\psi_s} \right)^{-1/b}, & \psi > \psi_s, \end{cases} \tag{5}$$

with θ_s the saturated moisture content [$\mathrm{m}^3\,\mathrm{m}^{-3}$], ψ_s the air-entry head [m], and b the Campbell exponent [-]; under hydrostatic equilibrium the suction at elevation z is $\psi = z - z_{\mathrm{wl}}$. Differentiating the storage components with respect to the water level gives the effective specific yield of the grid cell as the sum of a soil and a surface contribution,

$$S_{y,\mathrm{total}} = S_{y,\mathrm{soil}} + S_{y,\mathrm{surface}}. \tag{6}$$

Here $S_{y,\mathrm{soil}}$ is the spatially averaged soil specific yield [-]: through the $[1 - F_s]$ weighting in Eq. (4), it already accounts for how much non-inundated soil remains available to store water, so no further area weighting is applied (Dettmann and Bechtold, 2016). $S_{y,\mathrm{surface}}$ [-] is the surface (ponding) contribution: differentiating the surface-ponding storage (Eq. 3) with respect to the water level returns the cumulative elevation distribution evaluated at the water level, so the surface specific yield is exactly the inundated fraction of Eq. (2), $S_{y,\mathrm{surface}} = F_s(z_{\mathrm{wl}}) = F_{\mathrm{ponded}}$, which grows as the water level rises into the hollows. This flux partitioning assumes that the water level is horizontal across the grid cell, so that the soil column and the surface ponding stay in hydrostatic equilibrium and share a common water level at each time step. The fraction of each net surface flux directed to the soil column rather than to surface ponding is then

$$f_{\mathrm{soil}} = \frac{S_{y,\mathrm{soil}}}{S_{y,\mathrm{soil}} + S_{y,\mathrm{surface}}}. \tag{7}$$

Equivalently, $f_{\mathrm{soil}} = S_{y,\mathrm{soil}}/(S_{y,\mathrm{soil}} + F_s(z_{\mathrm{wl}}))$, so the complementary share routed to ponding, $1 - f_{\mathrm{soil}} = F_s(z_{\mathrm{wl}})/S_{y,\mathrm{total}}$, is the inundated fraction normalized by the total specific yield. When the water level is deep, $S_{y,\mathrm{surface}} \to 0$ and $f_{\mathrm{soil}} \approx 1$, so

https://doi.org/10.5194/egusphere-2026-5287
Preprint. Discussion started: 28 October 2026
© Author(s) 2026. CC BY 4.0 License.

water storage change occurs almost entirely within the soil. As the water level approaches or exceeds the surface, the inundated fraction and surface storage increase, f_{soil} [-] decreases, and a larger share of the net flux is stored as ponding.

Vertical water movement within the peat is solved in one dimension and does not depend on microtopography. The soil-water flux is written in suction form,

$$q_i = K_i \left(1 - \frac{\partial \psi_i}{\partial z}\right), \tag{8}$$

where K_i is the hydraulic conductivity $[\mathrm{m\,s^{-1}}]$; the first (unity) term is the gravitational contribution and the second is the suction-gradient contribution. This head-based form, rather than the moisture-gradient diffusion form of the default Noah-MP solver, avoids the artificial drainage that arises when a near-hydrostatic profile is represented on a coarse soil discretization: the moisture-based scheme cannot preserve the equilibrium state and generates spurious vertical fluxes when the water table sits within the column (Zeng and Decker, 2009). For shallow water levels (within 0.5 m of the surface), natural peatlands show negligible vertical gradients and the column is effectively at hydrostatic equilibrium (Bechtold et al., 2019; Dettmann and Bechtold, 2016); in this near-equilibrium regime the moisture-based solver is least able to reproduce the equilibrium profile and is most prone to these spurious fluxes and the associated numerical noise in the simulated water level, so the model bypasses it and instead updates the combined soil and surface storage directly under the hydrostatic assumption, then inverts the storage–water-level relationship to obtain the new water level. For deeper water levels, the full one-dimensional pressure-head Richards solution is retained. In both regimes the microtopographic factor f_{soil} couples the two domains: only the fraction f_{soil} of the net infiltration, evaporation, transpiration, and subsurface runoff acts on the soil column, while the complementary fraction $(1 - f_{\mathrm{soil}})$ is added to or released from surface ponding. However, evaporation from the ponded surface has not been accounted separately, and the evaporation for peat grid cells is still computed with the default Noah-MP resistance-based bare-soil formulation. The complete two-regime procedure, including the storage update, the water-level inversion, the mapping between the microtopography-averaged state and the one-dimensional column, and the treatment of saturated layers, is given in Appendix B with more details about the discretization in Fig. B1.

3.2.2 Peat soil hydraulic properties

The default Noah-MP STAS soil table (`NoahmpTable.TBL` in the refactored NoahMP v5.0) comprises 19 soil classes and does not include peat. We added peat as a new class, expanding the table to 20 classes. Rather than appending it as the last (20th) class, we inserted peat at index 17, immediately after the standard mineral and non-soil classes (1–16), and shifted the three rarely used special classes of the STAS scheme (playa, lava, and white sand) to indices 18–20, so that peat is grouped with the genuine soil classes. Because this reindexing changes the meaning of indices 17–20, users applying this study's soil-texture maps or LDT parameter files in other Noah-MP setups should pair them with the accompanying modified 20-class STAS table (rather than the standard 19-class table) to ensure that peat, playa, lava, and white-sand grid cells are assigned the correct hydraulic parameters. The peat water retention and hydraulic conductivity follow the Campbell–Clapp–Hornberger relations (Campbell, 1974; Clapp and Hornberger, 1978):

https://doi.org/10.5194/egusphere-2026-5287
Preprint. Discussion started: 28 October 2026
© Author(s) 2026. CC BY 4.0 License.

$$\psi(\theta) = \psi_s \left(\frac{\theta}{\theta_s} \right)^{-b} \tag{9}$$

$$K(\theta) = K_s \left(\frac{\theta}{\theta_s} \right)^{2b+3} \tag{10}$$

where, $K(\theta)$ is the unsaturated hydraulic conductivity [$\mathrm{m\,s^{-1}}$], K_s is the saturated hydraulic conductivity [$\mathrm{m\,s^{-1}}$], θ is the volumetric soil moisture content [$\mathrm{m^3\,m^{-3}}$], θ_s is the saturated soil moisture content [$\mathrm{m^3\,m^{-3}}$], $\psi(\theta)$ is the soil suction [m], ψ_s is the air-entry suction (saturated matric-potential magnitude) [m], and b is the Campbell–Clapp–Hornberger pore-size distribution exponent [-].

The peat matrix water-retention and hydraulic-conductivity parameters are vertically uniform and listed in Table 1. These parameters are calibrated for the Cuvette Centrale by Apers et al. (2026), using in-situ water level data for six well locations: three in Ekolongouma (SPT2,4,5) and three in Itanga (SPT3,5,6) and satellite-based precipitation by employing the Rise-and-Recession analysis method (Apers et al., 2025); and we transferred them directly into the Noah-MP parameter table `NoahmpTable.TBL`. Noah-MP additionally stores a saturated soil-water diffusivity (D_s, SATDW) for every soil class. The peat column, however, is advanced with the head-based solver (Eq. 8), which works in matric-potential form and therefore uses the hydraulic conductivity $K(\psi)$ directly rather than the moisture diffusivity; SATDW does not enter the peat hydrology and is retained only so that the peat class stays consistent with the table format expected by the default Noah-MP soil-water solver. For completeness, its value was obtained from the remaining peat parameters b, ψ_s, K_s, and θ_s following the standard relation

$$D_s = \frac{b\,|\psi_s|\,K_s}{\theta_s} \tag{11}$$

where ψ_s is the saturated soil matric potential (SATPSI) and b is the soil B parameter (BB). The dry soil-moisture threshold (DRYSMC) and the wilting-point soil moisture (WLTSMC) are taken from Liu et al. (2022). All peat soil parameters specified in `NoahmpTable.TBL` are listed in Table 1.

Table 1. Peat soil hydraulic properties

Properties	Fullname	Value
BB	Soil B parameter	7.9 [-]
DRYSMC	Dry soil moisture threshold	0.215 $\mathrm{m^3\,m^{-3}}$
MAXSMC	Saturated soil moisture	0.880 $\mathrm{m^3\,m^{-3}}$
REFSMC	Field capacity	0.6 $\mathrm{m^3\,m^{-3}}$
SATPSI	Saturated soil matric potential	0.049 m
SATDK	Saturated soil hydraulic conductivity	6.00×10^{-5} $\mathrm{m\,s^{-1}}$
SATDW	Saturated soil hydraulic diffusivity	2.64×10^{-5} $\mathrm{m^2\,s^{-1}}$
WLTSMC	Wilting point soil moisture	0.215 $\mathrm{m^3\,m^{-3}}$

https://doi.org/10.5194/egusphere-2026-5287
Preprint. Discussion started: 28 October 2026
© Author(s) 2026. CC BY 4.0 License.

Note that SATPSI (ψ_s) is tabulated as a positive magnitude throughout Noah-MP's parameter table (all 20 soil classes, peat included), following the original Noah LSM convention. The peat retention/suction formulation (Eq. 5, 9; implemented in `PeatMicroTopoMod.F90` and `SoilWaterDiffusionRichardsMod.F90`) uses ψ_s directly as this positive magnitude, consistent with the suction convention $\psi = z - z_{\mathrm{wl}}$ adopted here (Sect. 3.2.1).

3.2.3 Peatland runoff

The high saturated hydraulic conductivity of the peat macropores ($K_{s,macro}$) and the overall flat topography at the model grid scale allow all rainfall to infiltrate to the phreatic water level, so Hortonian runoff is negligible in peatlands (Bechtold et al., 2019; Apers et al., 2022, 2026). The total runoff (Q_{tot}) in natural tropical peatlands is low at lower water levels and increases non-linearly following a power law function (Romanov, 1968) with rising water levels, becoming very large when water breaches the surface in hollows and generates surface and subsurface runoff simultaneously. Following the same approach of Apers et al. (2026), we also introduced the empirical power law function of K. E. Ivanov (Romanov, 1968) for runoff discharge ($Q_{tot}(\overline{z}_{wl})$) in Noah-MP for the total runoff generation in the peatlands instead of Hortonian runoff. Physically, this water-level-dependent discharge represents the total lateral water export from the peatland and combines two near-surface pathways: shallow subsurface flow through the highly permeable, macropore-rich near-surface peat, and, as the water level rises into the hummock-hollow microtopography, slow overland flow across the partially inundated surface (Romanov, 1968; Baird, 1997; Kelly et al., 2014). The Ivanov transmissivity formulation lumps both pathways into a single water-level-dependent function rather than resolving them separately.

$$T_a(\overline{z}_{wl}) = \begin{cases} \dfrac{K_{s,macro,z=z_{max}-0.01}\,[100\,(z_{max}-\overline{z}_{wl})]^{1-\alpha}}{100(\alpha-1)}, & \text{for } \alpha>1,\ \overline{z}_{wl} < z_{max} \\ T_{a,max}, & \text{for } \alpha>1,\ \overline{z}_{wl} \geq z_{max} \end{cases} \tag{12}$$

$$Q_{tot}(\overline{z}_{wl}) = cT_a(\overline{z}_{wl}) \tag{13}$$

where, T_a is the transmissivity [$\mathrm{m^2\,s^{-1}}$], $\overline{z}_{wl}$ is the grid cell mean water level [m], $K_{s,macro,z=0-0.01}$ is the saturated hydraulic conductivity of the macropores evaluated just below the maximum water level [$\mathrm{m\,s^{-1}}$], α [-] is an empirical parameter that describes the rate of $K_{s,macro}$ decrease with depth, z_{max} [m] is the maximum water level above which the macropore transmissivity saturates, $T_{a,max}$ [$\mathrm{m^2\,s^{-1}}$] is this saturation value — a large, finite transmissivity that stands in for the formal $T_a \to \infty$ limit of Apers et al. (2026), implemented by capping the water level entering the transmissivity formula at $z_{\max} - \varepsilon$ ($\varepsilon = 10^{-4}$ m) for numerical stability, $Q_{tot}(\overline{z}_{wl})$ is the water level dependent runoff discharge [$\mathrm{m\,s^{-1}}$], and c is the average hydraulic gradient divided by the average length of the peatland in horizontal flow direction [$\mathrm{m^{-1}}$]. For the Cuvette Centrale, these parameters take the values $\alpha = 2.06$, $c = 1.5 \times 10^{-8}$ $\mathrm{m^{-1}}$, $K_{s,macro,z=z_{max}-0.01} = 3165.38$ $\mathrm{m^2\,s^{-1}}$, and $z_{max} = 0.245$ m. All these parameters have been derived from Apers et al. (2026), which employed the Congo-specific dis-

https://doi.org/10.5194/egusphere-2026-5287
Preprint. Discussion started: 28 October 2026
© Author(s) 2026. CC BY 4.0 License.

charge parameters for the Cuvette Centrale based on in-situ water-level recession behavior via satellite-precipitation-forced Rise-and-Recession analysis (Apers et al., 2025).

In the Noah-MP source code, we introduced the runoff function through a new module `RunoffSubSurfacePeatlandMod` for the peatland-specific runoff option (OptRunoffSubsurface=9). Because the scheme routes this combined discharge entirely through the model's subsurface-runoff component, the resulting flux is termed *subsurface runoff* only as a technical (code) designation: in reality, it is a mixed process of slow overland flow and near-surface matrix and macropore flow through the microtopography-dominated peatland surface.

We also modified the main soil-water balance module (`SoilWaterMainMod`) to suppress infiltration-excess (Hortonian) surface runoff on peat grid cells: the diagnosed surface runoff is added back to the infiltration term, consistent with the high macropore conductivity that allows rainfall to infiltrate or be stored in surface depressions rather than to form rapid overland flow. The rainfall is partitioned with the microtopographic factor f_{soil} between the soil column and surface ponding, as described in Sect. 3.2.1. The detailed handling of hydraulically active layers, subsurface-runoff removal, and the water-level cap at the column bottom is given in Appendix B.

3.2.4 Drought and waterlogging stress

Transpiration in tropical peatlands declines both at low water levels, through drought stress, and at high water levels, through waterlogging (Hirano et al., 2015). In PEATCLSM, these stress functions are derived from eddy-covariance evapotranspiration and water-level measurements (Apers et al., 2022). We follow the same approach in Noah-MP, combining the water-level-dependent waterlogging function of Apers et al. (2022) with the updated drought stress function calibrated for the Cuvette Centrale by Apers et al. (2026). Each of them is represented as a piecewise-linear function of the water level ($\overline{z}_{wl}$), defining two stress zones and one no-stress zone.

The drought stress factor F_{wilt} [-] represents the reduction in plant transpiration under declining water availability. When the water level is relatively shallow ($\overline{z}_{wl} > -0.3$ m), vegetation does not experience drought stress and the drought factor is set to zero. As the water level drops below this threshold, drought stress increases linearly with decreasing water level until reaching a maximum stress level when the water level exceeds -1.15 m (below surface). This behavior is implemented in the model using conditional statements that compute F_{wilt} as a segmented linear function of $\overline{z}_{wl}$, followed by bounding the value between 0 and 1 to ensure numerical stability.

$$F_{wilt} = \begin{cases} 0, & \text{if } \overline{z}_{wl} > -0.3 \\ -1.18\,\overline{z}_{wl} - 0.35, & \text{if } -0.3 \geq \overline{z}_{wl} > -1.15 \\ 1, & \text{if } \overline{z}_{wl} \leq -1.15 \end{cases} \tag{14}$$

https://doi.org/10.5194/egusphere-2026-5287
Preprint. Discussion started: 28 October 2026
© Author(s) 2026. CC BY 4.0 License.

The waterlogging stress factor F_{log} [-] represents limiting transpiration caused by high water levels. Note its reversed meaning relative to F_{wilt}, in line with Apers et al. (2022): F_{log} = 1 indicates no waterlogging stress, while F_{log} = 0 indicates maximum waterlogging stress.

When the water level remains below -0.29 m, plants experience no waterlogging stress, and the factor equals unity. As the water level rises toward the surface and above it, oxygen availability in the root zone decreases, reducing transpiration capacity. This reduction is represented as a linear decline in F_{log} between -0.29 m and 0.35 m water levels. Beyond 0.35 m the factor equals zero, representing maximum waterlogging conditions.

$$F_{log} = \begin{cases} 1, & \text{if } \overline{z}_{wl} \leq -0.29 \\ 1 - \dfrac{0.29 + \overline{z}_{wl}}{0.64}, & \text{if } -0.29 < \overline{z}_{wl} \leq 0.35 \\ 0, & \text{if } \overline{z}_{wl} > 0.35 \end{cases} \tag{15}$$

The drought and waterlogging stress functions are implemented in Noah-MP within the `SoilWaterTranspirationMod` routine, where transpiration limitation is computed based on the simulated water level. In the model code, we introduced a new soil-water transpiration option (OptSoilWaterTranspiration = 4) where these two stress components are diagnosed exclusively from the simulated water level as in PEATCLSM, rather than from layer-specific soil moisture and hydraulic conductivity. In the updated implementation, the drought and waterlogging factors are first combined into a bulk peatland stress term, β_{peat}, calculated as:

$$\beta_{\text{peat}} = (1 - F_{wilt}) F_{log} \tag{16}$$

Here β_{peat} [-] represents the overall reduction of transpiration due to the hydrological state of the peat column. In the code it is stored as the accumulated (bulk) transpiration factor that scales the total transpiration demand, while the vertical distribution of root-water uptake is set separately by a weight proportional to each layer's thickness within the root zone, so that the demand is drawn uniformly with depth across the root-zone layers. β_{peat} directly replaces the default Noah-MP soil-moisture transpiration factor (rather than being applied as an additional multiplier on top of it): when the peatland transpiration option is active, β_{peat} is assigned to the same bulk soil-water-stress variable that Noah-MP's stomatal resistance and photosynthesis schemes use for the default (Noah/CLM/SSiB) options, so no separate soil-moisture-based beta is computed in parallel.

A summary of all the changes made in the source code for implementing peatland hydrology is shown in Fig. 2.

https://doi.org/10.5194/egusphere-2026-5287
Preprint. Discussion started: 28 October 2026
© Author(s) 2026. CC BY 4.0 License.

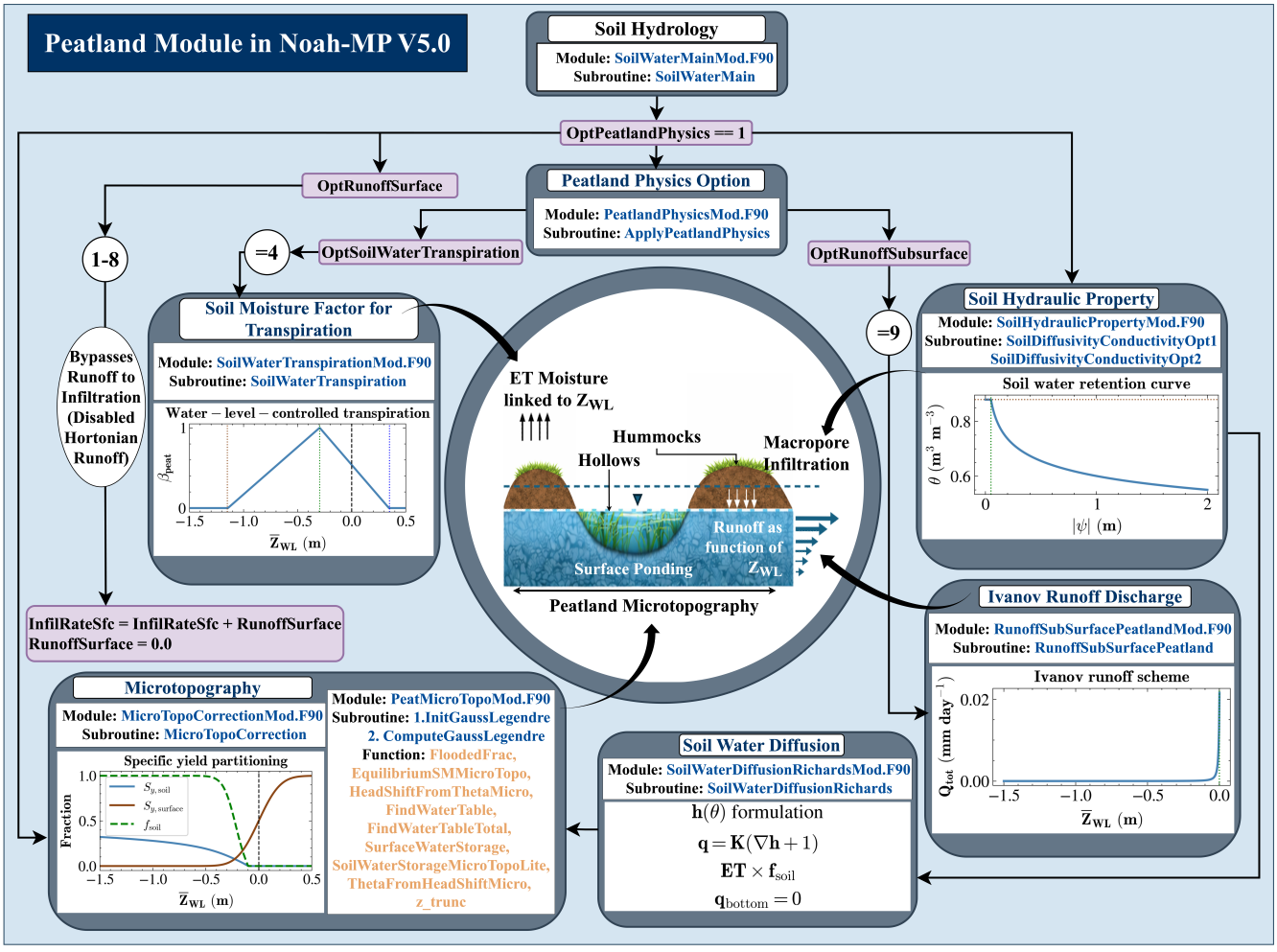


Figure 2. Summary of the peatland-specific modules and functions implemented in Noah-MP.

4 Experimental setup for model simulations

4.1 Meteorological forcings

The meteorological forcings for the Noah-MP experiments have been taken from two different sources. The Modern-Era Retrospective Analysis for Research and Applications, Version 2 (MERRA-2; Gelaro et al., 2017) is employed as the primary meteorological forcing dataset in this study. Developed by NASA's Global Modeling and Assimilation Office (GMAO), MERRA-2 provides a continuous record of atmospheric conditions from 1980 onward at a spatial resolution of 0.625° × 0.5° and an hourly temporal resolution.

https://doi.org/10.5194/egusphere-2026-5287
Preprint. Discussion started: 28 October 2026
© Author(s) 2026. CC BY 4.0 License.

Another data product is also used in this study specifically as a precipitation data source, obtained from the Climate Hazards Group InfraRed Precipitation with Station Data, Version 2 (CHIRPS v2; Funk et al., 2015). Developed by the Climate Hazards Center (CHC) at the University of California, Santa Barbara, CHIRPS provides global rainfall data covering the latitude band from 50°S to 50°N at a high spatial resolution of 0.05° from 1981 onwards. The dataset combines satellite-based infrared precipitation estimates with in-situ rain gauge observations and incorporates the Climate Hazards Group Precipitation Climatology (CHPclim) to improve the representation of long-term rainfall patterns. CHIRPS employs a multi-step blending procedure that integrates satellite observations, station measurements, and climatological information, including calibration against the Tropical Rainfall Measuring Mission (TRMM) Multi-Satellite Precipitation Analysis products.

The details of the forcing variables and their sources are shown in Table 2

Table 2. Meteorological forcing datasets used in Noah-MP experiments

Forcing Variable	Source	Specification
Precipitation	MERRA-2 (Gelaro et al., 2017)	0.625° × 0.5°
	CHIRPS (Funk et al., 2015)	0.05°
Other forcing variables (surface temperature, shortwave and longwave radiation, surface pressure, specific humidity, wind speed)	MERRA-2	0.625° × 0.5°

4.2 Model input parameters

For running Noah-MP within LIS, the framework needs the domain features like topography, land cover, soil texture, etc., embedded into an input NetCDF file. The NASA Land Data Toolkit (LDT; Arsenault et al., 2018) has been used for generating this domain and parameter data file containing all the model input features for LIS. LDT generates this input NetCDF file with a grid size of 0.1° × 0.1° by incorporating the model parameters of different resolutions enlisted in Table 3 using a remapping method appropriate to each dataset's resolution.

https://doi.org/10.5194/egusphere-2026-5287
Preprint. Discussion started: 28 October 2026
© Author(s) 2026. CC BY 4.0 License.

Table 3. LIS model parameter datasets and their specifications

Model Parameter	Source	Specification	Spatial transform
Digital elevation model	Multi-Error-Removed Improved-Terrain (MERIT) (Yamazaki et al., 2017)	90 m	Average
Land cover	MODIS IGBP land cover classes (Friedl et al., 2002) modified by National Centers for Environmental Prediction (NCEP)	0.0833°	Mode (Upscale by selecting dominant type for each grid cell)
Soil texture	FAO-derived soil texture map from Harmonized World Soil Database 1.21 (Fischer et al., 2008) processed by NCAR	5′	Mode
Congo peat map	Crezee et al. (2022)	50 m	Nearest neighbor
Greenness	NCEP (Gutman and Ignatov, 1998)	0.15°	Average
LAI and SAI	Monthly climatology processed from the Advanced Very High Resolution Radiometer (AVHRR) data by University of Maryland (Tian et al., 2008)	1 km	Average

4.3 Model experiment details

For this study, all the Noah-MP model simulations from 2010 to 2025 have been performed within the NASA Land Information System (LIS; Kumar et al., 2006, 2008; Peters-Lidard et al., 2007) framework version 7.5. Prior to this simulation period, the model was spun up by cycling a common 2000–2010 meteorological forcing period three times (three consecutive 10-year loops, each restarting from the previous cycle's end-of-year state), for a total of 30 years of spin-up, to equilibrate the slow-responding soil-moisture and peat water-storage states before the start of the reported simulations. This spin-up procedure was applied identically for the MERRA-2 and CHIRPS-forced configurations. LIS has been developed for high-performance terrestrial hydrology modeling and data assimilation to integrate satellite and ground-based observational data products and advanced modeling techniques to produce optimal estimates of land surface states and fluxes. LIS enables users to implement multiple land surface models, including Noah-MP, by taking various land surface and topographic inputs and meteorological forcings from multiple sources to simulate land surface processes and generate model states and fluxes at a consistent user-defined spatial resolution. In the model implementation, if the peatland physics option is turned on (OptPeatlandPhysics=1) in the global configuration, then the peatland module gets activated by enabling all the peatland hydrological functions described in Sect. 3.2. We restricted the peatland physics to peat pixels (soil type = 17) by adding a peatland map Crezee et al. (2022) as a new texture category "PEAT" in the LDT input file and by adding conditions in the LIS source code to trigger the peatland physics option for microtopography with peat soil properties and overwriting the default subsurface runoff option to OptRunoffSubsurface=9 with disabled Hortonian runoff and soil water transpiration to OptSoilWaterTranspiration=4 (Fig. 2) for those peat pixels only. The vegetation phenology follows the input-LAI configuration (dynamic vegetation option = 7, Table A1): monthly LAI and SAI climatologies are supplied via the LDT-generated input file rather than the default monthly values from the lookup table.

https://doi.org/10.5194/egusphere-2026-5287
Preprint. Discussion started: 28 October 2026
© Author(s) 2026. CC BY 4.0 License.

For the first set of simulations, the model takes all the meteorological forcings from MERRA-2. For the second case, the LIS setup is configured to use two meteorological forcing sources: MERRA-2 and CHIRPS (Table 2), with the blending option as "overlay". The MERRA-2 meteorological fields are read using the built-in MERRA-2 forcing readers and spatially interpolated using bilinear interpolation to the model grid. Similarly, CHIRPS precipitation data generated in LDT-readable format is also interpolated to the model grid. Within LIS, the overlay blending method gives precedence to the CHIRPS precipitation data. Consequently, CHIRPS precipitation from the LDT-generated forcing is used, and all non-precipitation variables are taken exclusively from MERRA-2.

For both of these forcing combinations, we performed four experiments (Experiment 1–4) across the two forcing sets with the peatland module off and on. With MERRA-2 forcing, the peatland module is turned off in Experiment-1 ($\text{NoahMP}_{\text{Peat=0,MER}}$) and turned on in Experiment-3 ($\text{NoahMP}_{\text{Peat=1,MER}}$); with CHIRPS precipitation, it is turned off in Experiment-2 (shown as $\text{NoahMP}_{\text{Peat=0,CH}}$) but turned on in Experiment-4 ($\text{NoahMP}_{\text{Peat=1,CH}}$). As a baseline experiment, we used the PEATCLSM outputs for the Congo peatlands forced with MERRA-2 from Apers et al. (2026), referred to as $\text{PEATCLSM}_{\text{MER}}$. The details of all these experiments are summarized in Table 4

Table 4. Summary of the experiment cases conducted within LIS for different forcing combinations in conjunction with the peatland physics module (on/off), with reference to PEATCLSM. Tick marks indicate the forcing source used for each variable in each experiment. Other forcing variables include shortwave and longwave radiation, surface pressure, specific humidity, and wind speed.

Forcing / configuration	**Experiment-1**		**Experiment-2**		**Experiment-3**		**Experiment-4**		**Baseline**	
	MERRA-2	**CHIRPS**	**MERRA-2**	**CHIRPS**	**MERRA-2**	**CHIRPS**	**MERRA-2**	**CHIRPS**	**MERRA-2**	**CHIRPS**
Precipitation	✓			✓	✓			✓	✓	
Other forcing variables	✓		✓		✓		✓		✓	
Model	Noah-MP		Noah-MP		Noah-MP		Noah-MP		CLSM	
Peatland physics module	Off		Off		On		On		On	
Acronym	$\text{NoahMP}_{\text{Peat=0,MER}}$		$\text{NoahMP}_{\text{Peat=0,CH}}$		$\text{NoahMP}_{\text{Peat=1,MER}}$		$\text{NoahMP}_{\text{Peat=1,CH}}$		$\text{PEATCLSM}_{\text{MER}}$	

The entire experimental setup is shown in the flowchart in Fig. 3.

https://doi.org/10.5194/egusphere-2026-5287
Preprint. Discussion started: 28 October 2026
© Author(s) 2026. CC BY 4.0 License.

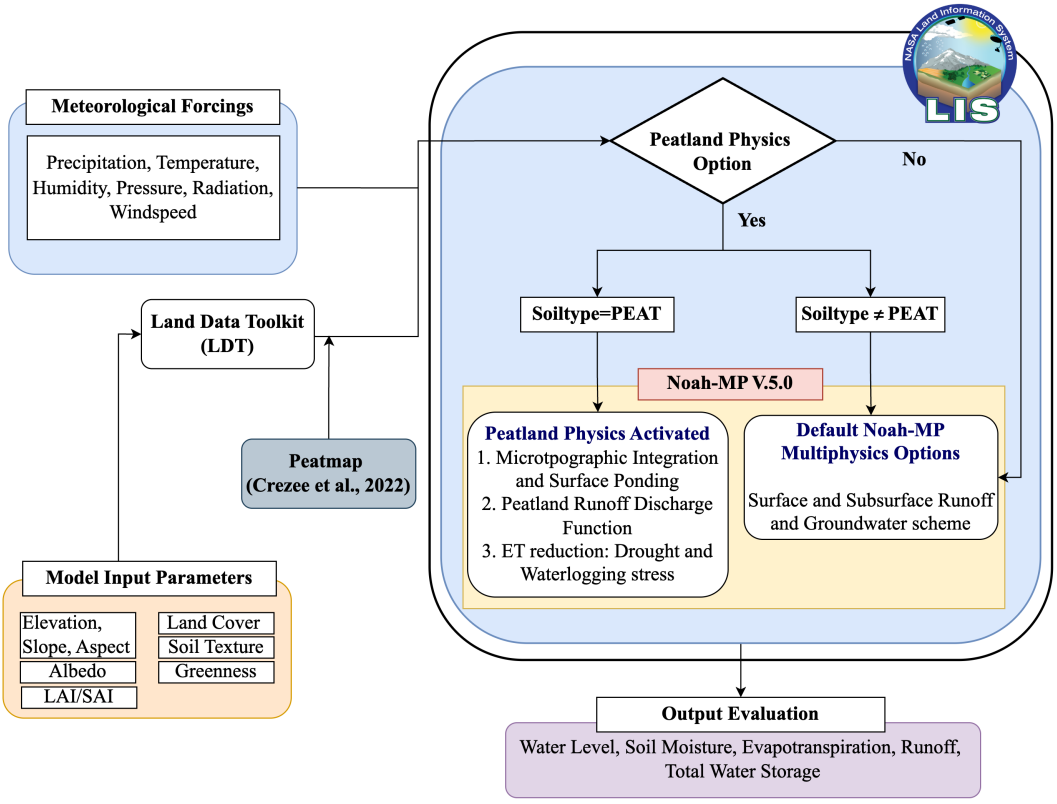


Figure 3. Methodology flowchart for the peatland module setup of Noah-MP and the experiments conducted within NASA LIS framework

5 Model performance evaluation: dataset and metrices

5.1 Evaluation datasets

5.1.1 In-situ water level data

This study uses in-situ water-level datasets collected from 20 well locations (Fig. 1) in the Cuvette Centrale peatland to evaluate model water-level outputs. The list of all well locations, their observation periods, and sources are tabulated in detail in Table C1.

5.1.2 Surface water elevation time series from satellite altimetry

This study also employs a satellite altimetry-based surface water elevation dataset, taken from the Database for Hydrological Time Series of Inland Waters (DAHITI; Schwatke et al., 2015), developed by the German Geodetic Research Institute at the Technical University of Munich (DGFI-TUM). Within the Cuvette Centrale study domain, DAHITI provides time series from 346 virtual stations across lakes, rivers, and wetlands (record length varies by station), derived from cross-calibrated altimetry

https://doi.org/10.5194/egusphere-2026-5287
Preprint. Discussion started: 28 October 2026
© Author(s) 2026. CC BY 4.0 License.

data (Envisat, ERS-2, Jason-1, Jason-2, TOPEX/Poseidon, SARAL/AltiKa, Sentinel-3, Sentinel-6MF) using a Kalman-filtering approach with extended outlier detection. DAHITI has been extensively used for various recent hydrological studies to understand the dynamics of inland water bodies and rivers (Busker et al., 2019; Scherer et al., 2022; Chen et al., 2025), along with the application in extending in-situ water level time series for data gap periods (Saemian et al., 2025). DAHITI dataset from 2010-2025 is used in this study in the calculation of the proxy surface water storage anomalies in conjunction with the river/lake hydrography dataset for surface water extent described in the following section.

.

5.1.3 Surface water extent dataset

To get the extent of the surface water and the river network in the Cuvette Centrale region, we employ the MERIT Hydro IHU (Eilander et al., 2021) global hydrography dataset, which is an upscaled version of the MERIT Hydro (Yamazaki et al., 2019) dataset using the Iterative Hydrography Upscaling (IHU) algorithm. It provides global maps of flow direction, river length, slope and width of river, along with elevation, stream order and upstream area. All these parameters, in conjunction with the DAHITI-derived altimetry water level dataset, are used to generate the surface water storage anomalies for the present study domain. Keeping consistency with the model resolution, the MERIT Hydro IHU product at 5 arcmin ($\sim$ 10 km) resolution has been chosen for this study. The entire surface water storage anomaly generation process using DAHITI and MERIT Hydro dataset is described in Sect. 5.2.

5.1.4 GRACE/GRACE-FO terrestrial water storage anomalies

The Gravity Recovery and Climate Experiment (GRACE; Tapley et al., 2004) and its successor, GRACE Follow-On (GRACE-FO; Landerer et al., 2020), offer precise measurements of changes in Earth's gravity field. The GRACE/GRACE-FO terrestrial water storage anomalies from the JPL GRACE and GRACE-FO Mascon Ocean, Ice, and Hydrology Equivalent Water Height Coastal Resolution Improvement (CRI) Filtered Release 06.3 Version 04 (JPL RL06.3M.MSCNv04; Wiese et al., 2023), covering the period from April 2002 to August 2025, are used in this study. This product is natively standardized by JPL to a 2004–2009 reference period; for comparison with the model output in this study, we additionally recenter all TWSA series (GRACE and model simulated) to a common 2010–2025 baseline, keeping consistency with DAHITI data and model outputs availability. Compared to spherical harmonic solutions, mass concentration (mascon) solutions offer less signal leakage and a higher spatial resolution (Wiese et al., 2016). Accordingly, no additional leakage/scale-factor correction is applied to the mascon time series used here. The Earth's surface in this approach is subdivided into customizable blocks or patches through a parameterization process, which are referred to as "mascons". The mass changes associated with each mascon are then estimated from gravity data. The JPL mascon grid product is released at a resolution of 0.5°, but the native resolution is the size of a single mascon, which is 3 degrees in size.

https://doi.org/10.5194/egusphere-2026-5287
Preprint. Discussion started: 28 October 2026
© Author(s) 2026. CC BY 4.0 License.

5.2 Dataset preprocessing

Available hydrological in-situ data for validation in the Cuvette Centrale are limited to phreatic water level observations. Water level is, however, the most influential hydrological variable in peatlands, is typically the most readily available, and it has accordingly been used for performance assessment here like other peatland modeling studies (Apers et al., 2022; Bechtold et al., 2019; Apers et al., 2026). All the well datasets have been resampled to daily scale to compare with the daily model outputs of water level.

Additionally, we evaluated the model performance in estimating total water storage anomalies (TWSA) by comparing against the GRACE/ GRACE-FO observations. Because by construction, neither Noah-MP nor PEATCLSM is subject to anthropogenic or hydrological trend forcings and does not reproduce long-term storage trends over the simulation period, we additionally remove a linear trend from the GRACE TWSA time series before computing the comparison statistics, so that the reported statistics reflect model skill in capturing interannual-to-seasonal variability rather than an unmodeled secular trend. The simulated series carry their own, generally small, secular drift (fitted linear trends of -0.04 to -0.30 cm yr^{-1} across the five configurations, versus GRACE's $+0.93$ cm yr^{-1}), which is non-negligible relative to GRACE's trend for the MERRA-2-forced configurations in particular; each simulated series is therefore also linearly detrended, independently, before the comparison statistics are computed, so that both sides of the comparison isolate interannual-to-seasonal variability from their own secular trend.

All model experiments conducted within LIS/Noah-MP give the vertically integrated water stored within land grid cells (e.g., soil moisture, groundwater, and water storage within the model landmask). On the other hand, the satellite-based gravimetric observations from GRACE capture the total water storage signal, which additionally includes contributions from surface water bodies. As the hydrodynamic model coupling is not done for the time being, the signal due to river water storage change is absent in the model-estimated land water storage anomalies (LWSA). Hence, the present study uses the DAHITI-based water level dataset in conjunction with the MERIT Hydro-based river network data described in Sect. 5.1.3 to generate the bulk signal of surface water storage anomalies (SWSA). The DAHITI virtual-station water surface elevation anomalies were interpolated onto the MERIT Hydro river network using a temporally and hydrologically constrained procedure. The length of the evaluation window is set by the shortest overlapping record among the compared products: from 2010 to 2025. DAHITI stations within the Cuvette Centrale domain were first restricted to the common baseline period 2010–2025, because many DAHITI records are sparse before 2010. A daily time axis was defined over this period, and each station series was linearly interpolated in time, while estimates farther than 45 days from the nearest observation were discarded to avoid filling long data gaps. River pixels were identified from MERIT Hydro using valid flow direction together with river width, upstream area, and stream order. Each DAHITI station was snapped to the nearest river cell within 20 km. The MERIT Hydro flow-direction field was then used to build a river-network, with river length defining along-channel distances between connected nodes. Spatial interpolation was carried out first by linear interpolation between consecutive upstream–downstream station pairs along the network, and subsequently by inverse-distance weighting based on shortest-path distances to fill remaining river nodes within each connected component. Water-level anomalies, referenced to the 2010–2025 mean at each station, were propagated through

https://doi.org/10.5194/egusphere-2026-5287
Preprint. Discussion started: 28 October 2026
© Author(s) 2026. CC BY 4.0 License.

this network to obtain a spatially continuous estimate of SWSA as representative of the bulk river contribution. This SWSA was added to the LSM-derived LWSA to obtain a more complete TWSA estimate comparable to the detrended GRACE time series. The sum of LWSA and SWSA as well as the GRACE TWSA, were referenced to a common 2010–2025 anomaly baseline by subtracting each grid cell's mean over that period, ensuring a zero-mean, consistent comparison.

5.3 Evaluation metrics

The model outputs have been evaluated using the following standard metrics. If $\bar{m}$ represents the mean estimates of a variable (e.g. water level, TWSA etc), and $\bar{o}$ represents the corresponding mean from the observation dataset then:

$$\bar{m} = \frac{1}{N}\sum_{i=1}^{N} m_i, \qquad \bar{o} = \frac{1}{N}\sum_{i=1}^{N} o_i \tag{17}$$

where m_i and o_i represent the model estimates and the observations for individual steps and N denotes the number of paired model-observation samples used in each comparison, and its size varies across evaluation targets: for the in-situ water-level comparisons it is set by each dip well's data-availability window and temporal coverage (Table C1), while for the GRACE-based TWSA comparison it is fixed by the number of valid monthly observations within the analysis period. Then the Pearson correlation (R) and Bias can be calculated as:

$$R = \frac{\sum_{i=1}^{N}(m_i - \bar{m})(o_i - \bar{o})}{\sqrt{\sum_{i=1}^{N}(m_i - \bar{m})^2}\sqrt{\sum_{i=1}^{N}(o_i - \bar{o})^2}} \tag{18}$$

$$\text{Bias} = \frac{1}{N}\sum_{i=1}^{N}(m_i - o_i) \tag{19}$$

The root mean squared error (RMSE) and the unbiased RMSE (ubRMSE) can be calculated as below:

$$\text{RMSE} = \sqrt{\frac{1}{N}\sum_{i=1}^{N}(m_i - o_i)^2} \tag{20}$$

$$\text{ubRMSE} = \sqrt{\text{RMSE}^2 - \text{Bias}^2} \tag{21}$$

6 Results

6.1 Process-level diagnostics

Prior to observation-based evaluation, we examined whether the peatland parameterizations produce physically consistent covariations among state and flux variables. The time series in Fig. 4a demonstrate that the peatland-specific processes in Noah-MP yield coherent dynamics among soil moisture, water level, and precipitation. The microtopography-based inundation

https://doi.org/10.5194/egusphere-2026-5287
Preprint. Discussion started: 28 October 2026
© Author(s) 2026. CC BY 4.0 License.

scheme allows the water level to rise above the mean surface elevation and fill subgrid hollows, as evidenced by periods in the time series when the water level rises above the surface (water level > 0; shaded region). The temporal evolution of soil moisture across the four layers (SM Layer 1-4) shows a coherent vertical response to water level fluctuations and precipitation forcing, with rapid saturation of the upper layers during wet periods. Conversely, during drying phases, the drawdown of the water level is accompanied by a progressive decline in soil moisture, with deeper layers retaining moisture longer, indicating proper representation of peat hydraulic properties and storage.

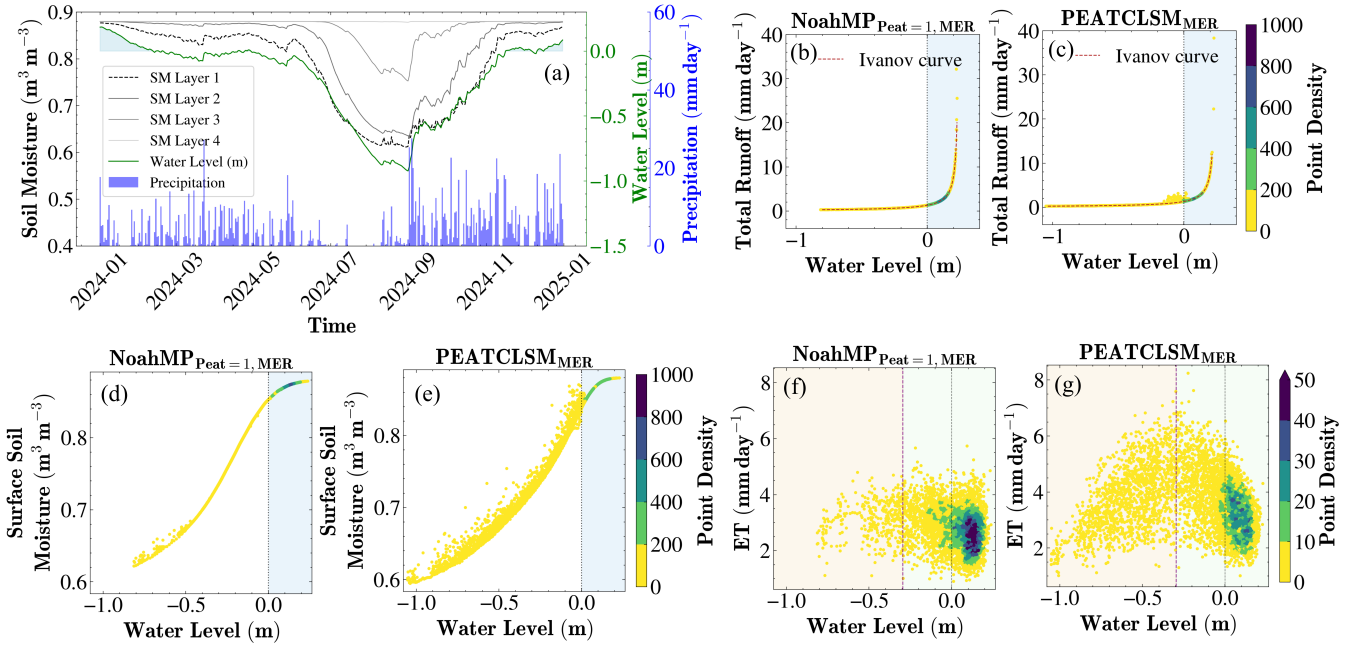


Figure 4. Process-level diagnostics of the peatland parameterizations implemented in Noah-MP. (a) Time series of water level, soil moisture across four model layers (SM layers 1-4), and precipitation for a representative peat grid cell (Mai-Ndombe) over 2024. Comparison of process-based functions between the Noah-MP peatland module ($\text{NoahMP}_{\text{Peat=1,MER}}$) and $\text{PEATCLSM}_{\text{MER}}$ from 2010 to 2025: (b–c) runoff discharge function – total runoff vs. water level, with the Ivanov transmissivity-decay curve — the model's imposed runoff function, not a statistical fit — overlaid (red dashed line); (d–e) surface soil moisture vs. water level; and (f–g) evapotranspiration response to water level, with the dry, transition, and waterlogging stress zones used in the ET formulation shown as shaded bands. In (b–g), each point represents one daily value; color encodes local point density, i.e., the number of days whose water level and response-variable pair fall within the same small neighborhood of the scatter, so that darker colors mark the most frequently occurring water-level-response combinations rather than isolated days. The light-blue shading in (b–c) and (d–e) marks water levels above the peat surface (water level > 0 m).

The water-level–runoff relationship (Fig. 4b–c) confirms that the runoff parameterization behaves as formulated. The point-density scatter plot shows a clear non-linear response, with negligible discharge under deep water level conditions and a rapid increase as the water level approaches the surface. Similarly, the relationship between ET and water level (Fig. 4f–g) shows a higher density of points for ET estimates corresponding to the ponding conditions (water level > 0), consistent with the

https://doi.org/10.5194/egusphere-2026-5287
Preprint. Discussion started: 28 October 2026
© Author(s) 2026. CC BY 4.0 License.

formulation of waterlogging stress, and decreasing ET at deeper water levels, consistent with drought stress. Variations in evaporation demands and in evaporation from intercepted water and soil cause the scatter in the relationship.

The basic operations of the peatland module of Noah-MP ($\text{NoahMP}_{\text{Peat}=1}$) and that of CLSM (PEATCLSM) were expected to be the same, as the theoretical basis of the peatland hydrological scheme, along with the identical parameterizations used for the peatland runoff discharge function. However, structural and other physics differences between the two models might lead to quantitative differences in the estimates of the key hydrological states, as evident from the comparative plots of the fundamental model states related to the peatland water level-dependent functions, for $\text{NoahMP}_{\text{Peat}=1,\text{MER}}$ and $\text{PEATCLSM}_{\text{MER}}$ in Fig. 4b–g. As both configurations essentially take meteorological inputs from the same forcing source (MERRA-2), it lays the foundation for a fair model structural comparison between their respective peatland schemes. Figure 4b–c compare the simulated runoff–water level relationship against the Ivanov transmissivity-decay curve – the model's imposed, not statistically fitted, runoff function – for $\text{NoahMP}_{\text{Peat}=1,\text{MER}}$ and $\text{PEATCLSM}_{\text{MER}}$, respectively. For $\text{NoahMP}_{\text{Peat}=1,\text{MER}}$, the scatter points closely follow the Ivanov curve, confirming that the implemented discharge function reproduces the intended Ivanov relationship. For $\text{PEATCLSM}_{\text{MER}}$, a few scatter points deviate from the curve's transition pattern at near-surface water levels. The extent of the curve along the x-axis also shows that PEATCLSM reaches comparatively deeper water levels (< -0.8 m) than Noah-MP.

The soil moisture–water level relationship (Fig. 4d–e) further strengthens the structural differences between PEATCLSM and $\text{NoahMP}_{\text{Peat}=1}$. In Noah-MP, soil moisture follows a tightly constrained, near-deterministic curve with water level, arising from its fixed multi-layer soil column and explicit vertical discretization. This leads to a strong and consistent coupling between water level and layer-wise soil moisture, with minimal scatter. Additionally, the surface ponding maintains persistently shallow water levels, resulting in a systematic shift of the curve toward wetter conditions (higher soil moisture for a given water level).

Furthermore, the relationships between ET and water level, presented as point-density scatter plots (Fig. 4f–g), contrast the two model behaviors under hydrological stresses. For both Noah-MP and PEATCLSM, the scatter points are mainly concentrated on the wet side, indicating that the site mostly faces waterlogging stress, which consequently leads to ET reduction. In fact, PEATCLSM ET shows a clear peak around -0.3 to -0.29 m, the narrow water-level band in which neither stress function is active ($F_{wilt} = 0$ and $F_{log} = 1$; Eq. 14 and 15). Moving toward shallower water levels from this point, waterlogging stress progressively increases (F_{log} declining to 0 by $z_{wl} = 0.35$ m, Eq. 15); moving toward deeper water levels, drought stress progressively increases (F_{wilt} rising to 1 by $z_{wl} = -1.15$ m, Eq. 14). A substantial fraction of scatter points occupies this broader transition envelope (z_{wl} between -1.15 and 0.35 m), where at most one of the two stresses is partially active rather than both simultaneously minimized, resulting in a wide spread of ET values and frequent occurrences of elevated ET (> 5 mm day^{-1}) in PEATCLSM results. However, $\text{NoahMP}_{\text{Peat}=1}$ shows a more constrained distribution, with most scatter points clustered near shallow water levels (> -0.3 m), where waterlogging stress dominates and suppresses ET. Consequently, high ET values are less frequent and the overall variability is reduced.

https://doi.org/10.5194/egusphere-2026-5287
Preprint. Discussion started: 28 October 2026
© Author(s) 2026. CC BY 4.0 License.

6.2 Spatiotemporal evaluation of changes in soil–water dynamics relative to reference models

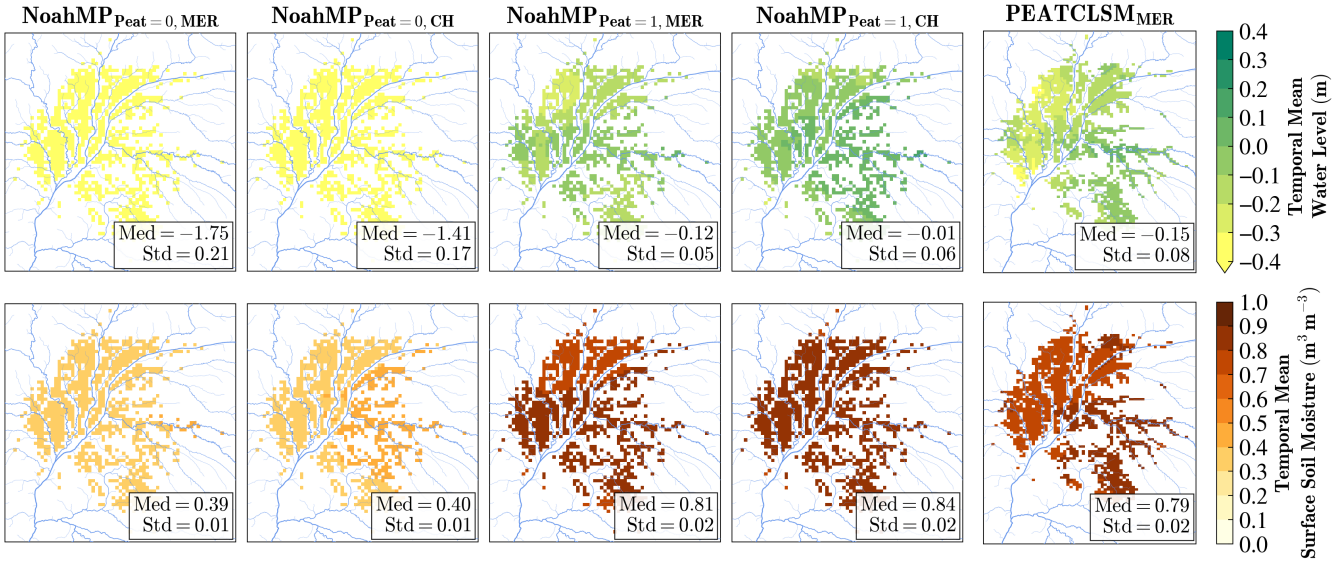


Figure 5. Maps of temporal mean water level and mean surface soil moisture for the time period 2010-2025 over the Cuvette Centrale peatlands; the overall spatial spread/distribution is expressed in terms of spatial median (Med) and standard deviation (Std).

The spatial patterns of temporal mean water level and surface soil moisture reveal a systematic sensitivity to both peatland physics activation and meteorological forcing in Fig. 5. When peatland physics options are disabled ($\text{NoahMP}_{\text{Peat}=0}$), the model simulates consistently deep water levels (median = -1.75 m for MER and -1.41 m for CH) and low surface soil moisture (0.39–0.40 $\text{m}^3\ \text{m}^{-3}$).

In contrast, activation of peatland physics ($\text{NoahMP}_{\text{Peat}=1}$) leads to a substantial rise in water level (median = -0.12 m for MER and -0.01 m for CH) and higher soil moisture (0.81–0.84 $\text{m}^3\ \text{m}^{-3}$). Across forcings, CHIRPS-driven simulations consistently produce shallower water levels and higher soil moisture than MERRA-2, indicating stronger effective precipitation input and higher infiltration. Among all configurations, $\text{NoahMP}_{\text{Peat}=1,\text{CH}}$ exhibits the wettest conditions, with near-surface water levels and high peat moisture contents near saturation. The PEATCLSM reference shows comparable wet conditions (median water level of about -0.15 m and soil moisture of about 0.79 $\text{m}^3\ \text{m}^{-3}$), but with slightly greater spatial heterogeneity than $\text{NoahMP}_{\text{Peat}=1}$.

6.3 Evapotranspiration regulation under hydrological stress

The spatial patterns of evapotranspiration presented in Fig. 6 reveal a clear signature of the water level-controlled ET reduction function implemented in the peatland simulations. Across all configurations, ET is strongly constrained within a relatively narrow range ($\sim$ 2–4 mm day^{-1}), but systematic shifts in both the spatial magnitude and distribution emerge depending on model physics and forcing as evident from the median and standard deviation values.

https://doi.org/10.5194/egusphere-2026-5287
Preprint. Discussion started: 28 October 2026
© Author(s) 2026. CC BY 4.0 License.

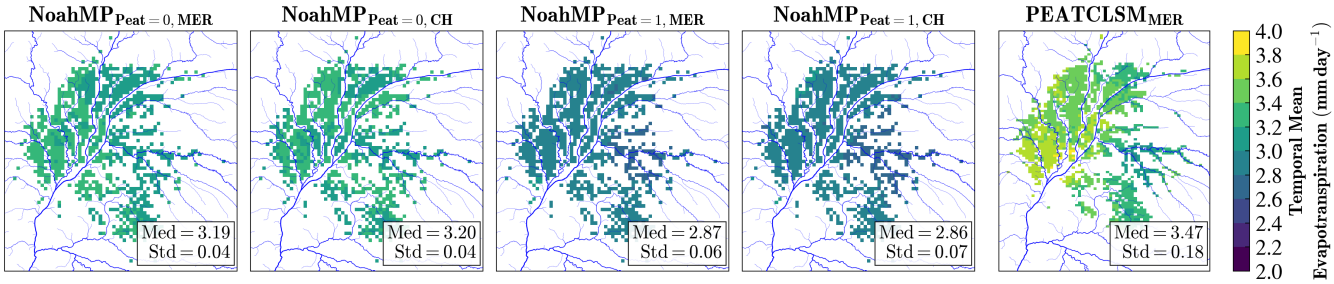


Figure 6. Spatial maps of evapotranspiration along with their distribution in terms of density plots for the peat pixels

When the peatland processes are not incorporated ($\text{NoahMP}_{\text{Peat}=0}$), comparatively symmetric spatial distributions of ET can be observed centered around 3 mm day^{-1} with slightly higher median values (median = 3.19–3.20 mm day^{-1}) for both MERRA-2 and CHIRPS. Whereas, activating peatland physics ($\text{NoahMP}_{\text{Peat}=1}$) leads to a consistent reduction in median ET (median = 2.86–2.87 mm day^{-1}) in comparison to default model results under both the forcings. However, based on spatial maps, the $\text{NoahMP}_{\text{Peat}=1}$ simulated water level remains close to the surface most of the time, leading to frequent waterlogging conditions, limiting transpiration, thereby lowering ET.

On the contrary, the PEATCLSM estimated ET displays a contrasting behavior, with a higher median ET (median of 3.47 mm day^{-1}) and a broader distribution extending toward values even higher than the default Noah-MP runs (> 3 mm day^{-1}). This model behavior can be understood in terms of how the two models deal with bare soil evaporation and plant transpiration, discussed in Sect. 7.3 later.

6.4 Runoff generation controlled by water level

The spatial variability of surface and subsurface runoff over the peat pixels (Fig. 7) clearly reflects the impact of peatland hydrological processes, particularly the implementation of the Ivanov-based subsurface runoff scheme and the suppression of Hortonian (infiltration-excess) runoff. In the absence of peatland physics ($\text{NoahMP}_{\text{Peat}=0}$), surface runoff dominates the hydrological response, with relatively high median values (0.46–0.51 mm day^{-1}) and pronounced spatial variability. In contrast, subsurface runoff remains comparatively low (0.97–1.02 mm day^{-1}), indicating that excess water is primarily routed as overland flow, consistent with the usual characteristic of Hortonian runoff generation.

https://doi.org/10.5194/egusphere-2026-5287
Preprint. Discussion started: 28 October 2026
© Author(s) 2026. CC BY 4.0 License.

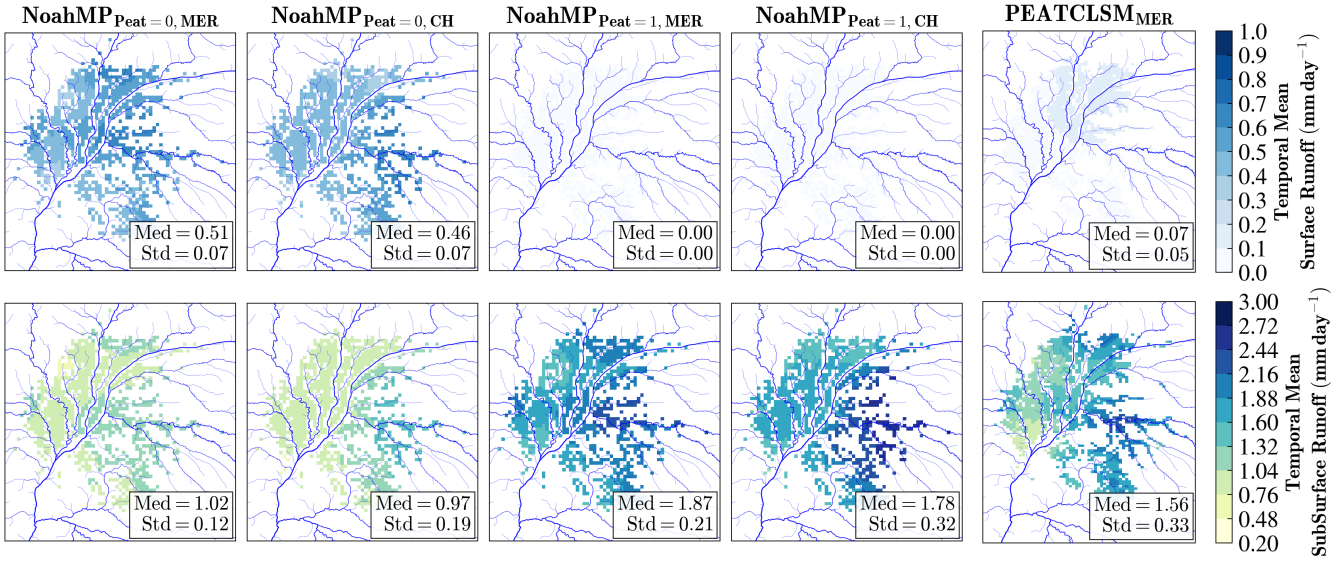


Figure 7. Spatial maps of surface and subsurface runoff obtained from the different model configurations for the peat pixels of the Cuvette Centrale region

When peatland physics is turned on ($\text{NoahMP}_{\text{Peat}=1}$) surface runoff is almost entirely suppressed (median close to 0.00 mm day^{-1}), consistent with the deactivation of Hortonian runoff and the high infiltration capacity of peat macropores. Instead, runoff is predominantly generated as subsurface flow, as evident from the higher median values (1.78–1.87 mm day^{-1}). Keeping consistency with the water level estimates, CHIRPS-forced simulations exhibit comparatively higher subsurface runoff. Like shallow water level, $\text{NoahMP}_{\text{Peat}=1,\text{CH}}$ also produces the strongest subsurface runoff signal, reflecting the combined effect of high water availability and saturation-driven flow. The PEATCLSM reference shows a similar dominance of subsurface runoff (median = 1.56 mm day^{-1}) and weak surface runoff (0.07 mm day^{-1}), confirming that peatland hydrology is primarily governed by saturation-excess and catchment deficit mechanisms in CLSM, in contrast to $\text{NoahMP}_{\text{Peat}=1}$ that has multi-layer soil water dynamics representation. This is evident from the lower subsurface runoff and greater spatial heterogeneity in PEATCLSM estimates.

https://doi.org/10.5194/egusphere-2026-5287
Preprint. Discussion started: 28 October 2026
© Author(s) 2026. CC BY 4.0 License.

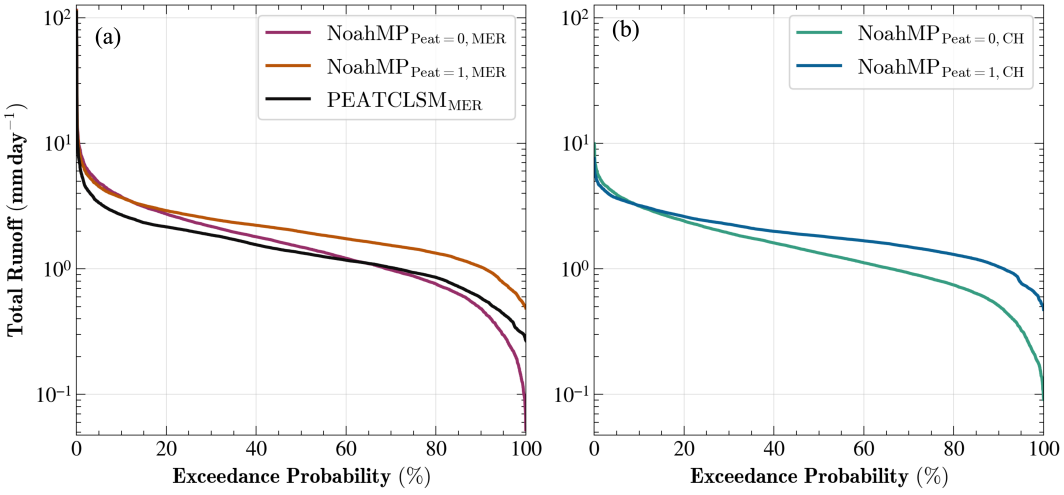


Figure 8. Empirical flow duration curves (FDCs) of daily total runoff (surface + subsurface/baseflow) for the peat pixels, 2010–2025, under (a) MERRA-2 and (b) CHIRPS precipitation forcing. Each curve is the empirical distribution — every ranked daily, peat-averaged runoff value plotted at its Weibull exceedance probability (see equation above) — with no parametric curve fit applied. Panel (a) compares three MERRA-2-forced configurations: NoahMP$_{\mathrm{Peat=0,MER}}$ (default Noah-MP), NoahMP$_{\mathrm{Peat=1,MER}}$ (peatland parameterization active), and PEATCLSM$_{\mathrm{MER}}$. Panel (b) compares the two CHIRPS-forced Noah-MP configurations, NoahMP$_{\mathrm{Peat=0,CH}}$ and NoahMP$_{\mathrm{Peat=1,CH}}$; PEATCLSM was run only under MERRA-2 forcing and is therefore not shown in (b)

Figure 8 shows the flow duration curve (FDC) of daily total runoff (surface + subsurface/baseflow), summarizing the full distribution of runoff magnitudes, from rare high-flow events (low exceedance probability, P) to persistent low flows (high P), and its low-flow tail is the key hydrological diagnostic of the Cuvette Centrale peatland's water-storage and release behavior. For this purpose, the daily total runoff is spatially averaged over the peat grid cells, sorted in descending order, and assigned a Weibull exceedance probability function, $P = 100 \times \frac{\mathrm{rank}}{n+1}$, where rank is the position in the ordered series and n is the total number of observations. Here, it is shown to isolate how the retention capacity of peat reshapes the balance between flashy surface runoff and sustained baseflow.

First of all, Fig. 8 reveals that activating the peatland parameterization (NoahMP$_{\mathrm{Peat=1}}$) systematically increases total runoff relative to the default Noah-MP configuration (NoahMP$_{\mathrm{Peat=0}}$) across most exceedance probabilities under both precipitation forcings. The largest differences occur in the low-flow regime (P = 60–100 %), while the curves converge during extreme runoff events. The enhanced runoff persistence is observed in all NoahMP$_{\mathrm{Peat=1}}$ configurations indicating hydrological connectivity and enhanced baseflow contribution. Second, precipitation forcing strongly influences the upper portion of the flow-duration curve. MERRA-2 produces a higher and steeper high-flow tail than CHIRPS, indicating more intense runoff-generating events, whereas CHIRPS yields a smoother runoff distribution. Under identical MERRA-2 forcing, PEATCLSM remains closer to NoahMP$_{\mathrm{Peat=0}}$ than to NoahMP$_{\mathrm{Peat=1}}$ across the low-to-median flow range. While both peatland models simulate enhanced

https://doi.org/10.5194/egusphere-2026-5287
Preprint. Discussion started: 28 October 2026
© Author(s) 2026. CC BY 4.0 License.

runoff persistence relative to the default Noah-MP configuration, $\text{NoahMP}_{\text{Peat}=1}$ generates larger sustained runoff, reflecting differences in model structure and physics.

6.5 Evaluation with observation datasets

6.5.1 Statistical analysis with in-situ water level data

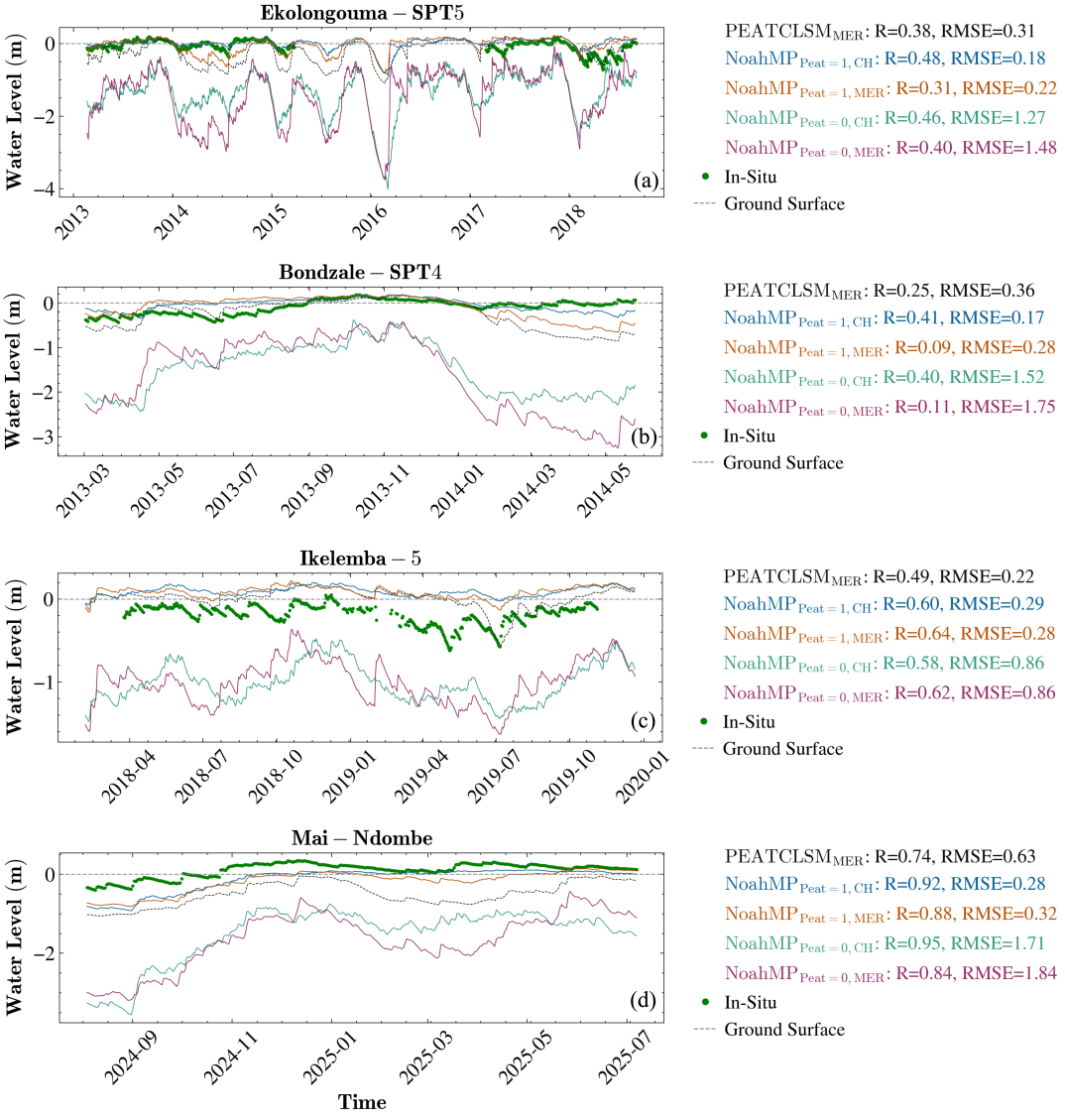


Figure 9. Comparison of peat water level time series from different model configurations with in-situ data across four well locations: (a) Ekolongouma-SPT5, (b) Bondzale-SPT4, (c) Ikelemba-5, and (d) Mai-Ndombe. The respective values of correlation and RMSE in 'm' with the in-situ data are shown in the legend.

https://doi.org/10.5194/egusphere-2026-5287
Preprint. Discussion started: 28 October 2026
© Author(s) 2026. CC BY 4.0 License.

Figure 9 compares simulated and observed water level time series exemplarily at four monitoring wells. It is observed that the peat-enabled configurations ($\text{NoahMP}_{\text{Peat=1}}$) capture the temporal variability of water level dynamics better than their non-peat counterparts and, at many sites, also better than PEATCLSM. At Ekolongouma (Fig. 9a) and Bondzale (Fig. 9b), $\text{NoahMP}_{\text{Peat=1,CH}}$ achieves higher correlations ($\text{R} = 0.48$ and 0.41, respectively) and lower RMSE ($\text{RMSE} = 0.18$ and 0.17, respectively) than PEATCLSM, indicating a better representation of seasonal fluctuations and short-term variability. At Ikelemba-5 (Fig. 9c), $\text{NoahMP}_{\text{Peat=1,MER}}$ shows the highest correlation ($\text{R} = 0.64$). At Mai-Ndombe (Fig. 9d), the site with the latest available records, CHIRPS-driven outputs show the best overall agreement with in-situ data (R up to 0.92 and 0.95, for peat and no-peat cases, respectively), outperforming both MERRA-2-driven configurations of Noah-MP and PEATCLSM. However, the overall domain wide model performance can be well understood from the statistics across all well locations, summarized in Table C2.

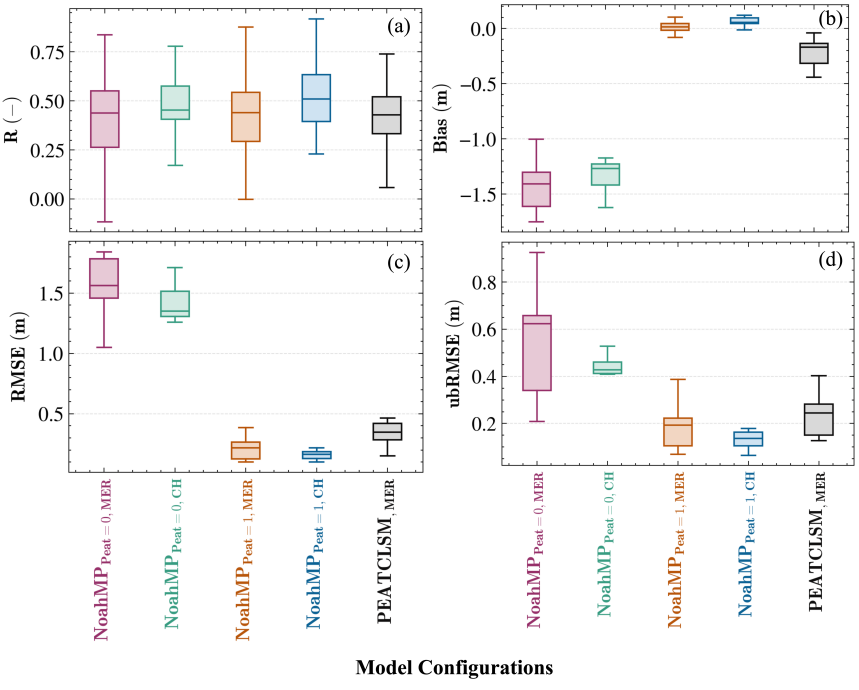


Figure 10. Boxplots of the statistical metrics for all the model configurations in estimating water level in comparison with in-situ well data.

The box plots in Fig. 10 summarize the overall performance of all model configurations across the in-situ wells (Table C2). Both peat-enabled simulations ($\text{NoahMP}_{\text{Peat=1}}$) exhibit higher correlations, near-zero bias, and substantially reduced RMSE and ubRMSE compared to their non-peat counterparts ($\text{NoahMP}_{\text{Peat=0}}$), which suffer from strong negative bias and large errors. Among all configurations, $\text{NoahMP}_{\text{Peat=1,CH}}$ shows best overall performance, showing slightly higher median R and the lowest median RMSE and ubRMSE, along with minimal bias. $\text{NoahMP}_{\text{Peat=1,MER}}$ also performs well but is slightly

https://doi.org/10.5194/egusphere-2026-5287
Preprint. Discussion started: 28 October 2026
© Author(s) 2026. CC BY 4.0 License.

inferior to NoahMP$_{\mathrm{Peat=1,CH}}$. Compared to the reference PEATCLSM$_{\mathrm{MER}}$ simulation, both peat-enabled Noah-MP runs demonstrate clear improvements, particularly in reducing RMSE, ubRMSE and bias.

6.5.2 Total water storage dynamics evaluation with GRACE

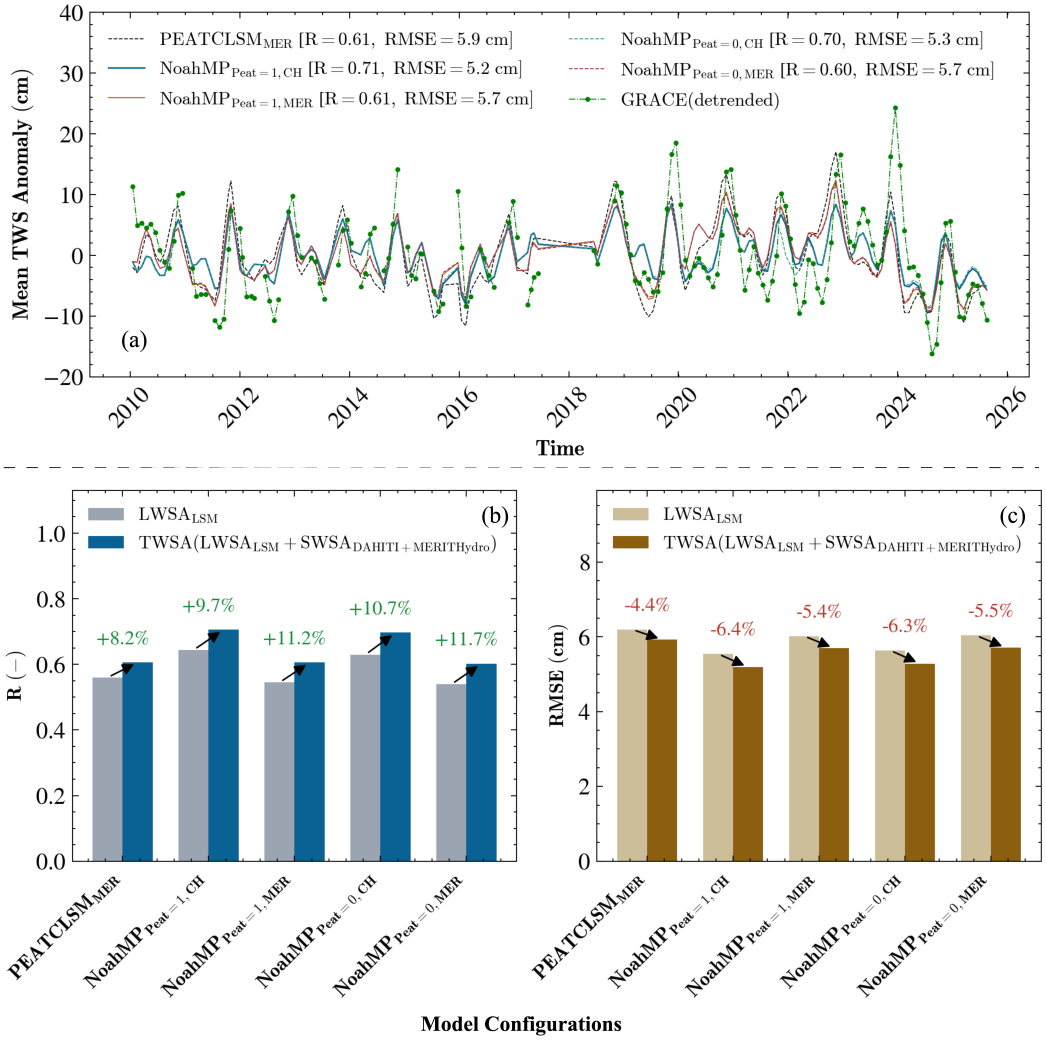


Figure 11. Total water storage anomaly (TWSA) evaluation against GRACE over the full Cuvette Centrale domain (peat and non-peat pixels combined), 2010-2025 baseline. (a) Spatial-mean time series of TWSA [= land water storage anomaly (LWSA$_{\mathrm{LSM}}$) plus the DAHITI+MERIT-Hydro-derived surface water storage anomaly (SWSA$_{\mathrm{DAHITI+MERITHydro}}$)] for all five model configurations, compared against detrended GRACE TWSA. (b–c) Effect of adding the SWSA correction on agreement with GRACE for each configuration: (b) Pearson correlation (R) and (c) RMSE (cm), each shown for the land-storage-only estimate (LWSA$_{\mathrm{LSM}}$, lighter bars) and for the combined estimate (TWSA, darker bars); the percentage above each bar pair gives the relative change in R or RMSE from adding the SWSA correction.

https://doi.org/10.5194/egusphere-2026-5287
Preprint. Discussion started: 28 October 2026
© Author(s) 2026. CC BY 4.0 License.

The comparison of domain-averaged time series of model-estimated total water storage anomalies (TWSA), comprising both peat and non-peat pixels, highlights the contribution of river/surface water storage to reproducing GRACE-observed TWSA. Figure 11a compares the time series of the combined total water storage anomaly (TWSA) — land storage plus the proxy surface water storage anomaly — from different model configurations with the GRACE TWSA time series. From the time series, it is evident that all configurations reproduce the seasonal cycle reasonably well.

Figure 11b–c quantify the effect of adding the DAHITI+MERIT-Hydro-derived surface water storage anomaly (shown as $\mathrm{SWSA_{DAHITI+MERITHydro}}$) to the land-only storage estimate ($\mathrm{LWSA_{LSM}}$) for each configuration. When this proxy surface water storage anomaly derived from DAHITI altimetry is added, the agreement with GRACE improves marginally across all configurations, with correlations (R) increasing by up to 11.7% and RMSE reducing by 6.4%.

On the other hand for the LSM-only case ($\mathrm{LWSA_{LSM}}$) in Fig. 11, all these configurations show relatively low correlations and higher RMSE. This limitation arises because LSMs represent only terrestrial water storage (soil moisture, groundwater, and canopy water) and do not simulate the streamflow dynamics. Among all the configurations, $\mathrm{NoahMP_{Peat=1,CH}}$ consistently shows the relatively better performance with highest correlation ($\mathrm{R} = 0.64$–0.71) and lowest RMSE ($\mathrm{RMSE} = 5.19$–5.54 cm), indicating the possibility of further enhancement in the representation of total storage variability with the new peatland module by assimilating GRACE TWSA observations with better precipitation input.

7 Discussion

This paper presents the implementation and evaluation of peatland hydrological processes in Noah-MP version 5.0 over the Cuvette Centrale peatland complex. The spatial dynamics, model consistency, and temporal evaluation have shown promising results from the peatland hydrology parameterizations throughout the entire Sect. 6. In fact, the statistical evaluation using in-situ water level data in Sect. 6.5.1 consistently shows that incorporating the peatland physics in Noah-MP substantially improves model performance. However, certain insights from these results can be further inferred and discussed in detail, especially focusing on the inherent physical processes considering the quality and limited availability of data products for robust evaluation.

7.1 Hydrological controls and model performance

The Noah-MP model with the newly introduced peatland parameterization estimates wetter conditions relative to the default model setup as indicated by shallow water level and higher soil moisture (Fig. 5), potentially reflecting the impacts of incorporating the microtopography parameterization with peat soil properties. The reduced ET (Fig. 6) estimated by the peatland scheme is a direct consequence of the water level constrained reduction function, which suppresses transpiration consistent with the frequent waterlogging behavior of Congo peatlands.

Peatland physics suppresses the surface runoff, and the total runoff generation is dominated by an increased subsurface flow as a mixed process of combined slow overland and matrix flow through the microtopography-dominated peatland surface. As the water level rises to near the surface, as shown in the spatial water level patterns in Fig. 5, lateral drainage and

https://doi.org/10.5194/egusphere-2026-5287
Preprint. Discussion started: 28 October 2026
© Author(s) 2026. CC BY 4.0 License.

saturation-excess processes dominate, producing spatially coherent subsurface runoff patterns that closely follow spatial patterns of absolute wetness, i.e., shallow water level over peatlands.

The patterns of the flow duration curves of daily total runoff (Fig. 8) further confirm consistent hydrological behavior of peatlands as systems with high storage capacity and more baseflow contribution, promoting a more buffered seasonal response, with water being stored during wet periods and released more gradually thereafter. This model realization reflects the effect of peat macropore infiltration and the Ivanov-based formulation where runoff is controlled by water level and soil saturation rather than infiltration excess. Whereas the curves converge during extreme runoff events, indicating that peak flows are primarily controlled by precipitation intensity.

7.2 Impact of precipitation inputs

The use of two different input precipitation as model forcings (MERRA-2 and CHIRPS) implies that the peatland physics implementation is the primary control on the hydrological states, while input precipitation just regulates the magnitude of wetness, with CHIRPS forcing providing an additional performance gain along with peatland physics. MERRA-2 produces a higher and steeper high-flow tail than CHIRPS (Fig. 8), indicating more intense runoff-generating events, whereas CHIRPS yields a smoother runoff distribution. Although the statistical evaluation in Sect. 6.5 shows substantial improvement in model performance across all the forcings due to the inclusion of peat parameterizations in comparison to their corresponding default model setup, CHIRPS-forced simulations consistently outperform the results of MERRA-2 forced simulations.

Part of the improved skill metrics with CHIRPS at station locations may, however, reflect an effective-resolution artifact rather than a purely superior representation of precipitation processes. MERRA-2-driven ($0.625° \times 0.5°$) simulations are, by design, unable to reproduce subgrid-scale variability at point-scale even after getting interpolated bilinearly onto the finer $0.1°$ model grid regardless of how accurate the areal-mean MERRA-2 rainfall estimate is. In-situ validation will therefore inherently favor a forcing product with finer effective resolution (CHIRPS $0.05°$).

Unlike the station-based comparisons discussed above, the GRACE TWSA evaluation in Fig. 11 is performed on domain-averaged (spatial mean) time series over the full Cuvette Centrale domain which integrates out subgrid-scale variability. So the resolution-driven mechanism invoked to explain the advantage of using CHIRPS at station level cannot account for its improved agreement with GRACE here. The persistence of a CHIRPS-driven improvement in this domain-integrated setting therefore points to a genuine difference in the domain-total precipitation amount, seasonal timing, or bias between the two forcing products, rather than a resolution artifact – providing independent support that CHIRPS offers a quantitatively more accurate precipitation input for this region, and not merely a higher-resolution one. This is consistent with independent evaluations of precipitation products over Africa and the Congo Basin, which similarly report CHIRPS to outperform reanalysis-based products such as MERRA-2 (Kouakou et al., 2023; Dos Santos et al., 2022; Dinku et al., 2018).

7.3 Model differences: Noah-MP Peat vs PEATCLSM

Despite employing the same soil hydraulic parameter-based runoff scheme and water-level-based drought/waterlogging stress functions as PEATCLSM in the Noah-MP peatland module, the comparative process-based plots in Fig. 4 show different

https://doi.org/10.5194/egusphere-2026-5287
Preprint. Discussion started: 28 October 2026
© Author(s) 2026. CC BY 4.0 License.

runoff and ET distributions with respect to water level. The first and foremost reason can be attributed to the direct impact of differences in water level dynamics, considering the fact that both these functions are dependent on water level fluctuation. As indicated by the spatial patterns of water level (Fig. 5), PEATCLSM tends to produce comparatively deeper water levels across large portions of the domain than Noah-MP, resulting in a substantial fraction of grid cells falling within the transitional to drought stress range (-0.3 to -1.15 m) based on the thresholds set in Eq. 14, as evident from Fig. 4f–g, and shows peak ET within -0.29 to -0.30 m regime, where neither waterlogging nor drought stress is dominant. This leads to a systematic increase in moderate-to-high ET values from PEATCLSM, thereby widening the spread of distribution and shifting its central tendency toward higher values (Fig. 6). For the same reason, the water level dependent runoff dynamics also differ between these two models (Fig. 4b–c). The differences in microtopographic representation have direct implications for the simulated water level dynamics. As already mentioned in Sect. 3.2.1, in PEATCLSM, although based on the same theory of Dettmann and Bechtold (2016), the ponded fraction is approximated empirically as a function of water level using the operational functions of CLSM (Koster et al., 2000; Ducharne et al., 2000). In contrast, the discretized microtopography scheme implemented in Noah-MP v5.0, based on Dettmann and Bechtold (2016), introduces explicitly the subgrid elevation distribution, which better represents the storage–water level relationship. The statistical evaluation in Sect. 6.5.1 further confirms these trends, with median improvements across all metrics (Fig. 10) in Noah-MP peatland module.

Additionally, there are certain model structural and physics differences in the two LSMs which might have led to the difference in their ET estimates. Despite having a common resistance-based, Penman-Monteith/SiB theoretical basis (Sellers, 1985), CLSM and Noah-MP differ substantially in the surface energy balance scheme. CLSM represents vegetation and soil as a single composite surface per soil-moisture regime, whereas Noah-MP resolves separate canopy, snow, and soil components as well as their coupling within ground energy balances, which are linked through a shared canopy-air layer, allowing radiative, turbulent, and longwave exchanges to be partitioned asymmetrically between vegetation and soil rather than lumped together. In CLSM soil hydraulic and thermal properties are prescribed from continuous, pre-processed parameter fields, while Noah-MP assigns them from discrete soil-texture classes via pedotransfer-based lookup tables (Cosby et al., 1984). Canopy conductance in CLSM follows an empirical Jarvis-type formulation driven by radiation, temperature, and soil-moisture stress with no sensitivity to atmospheric CO_2, whereas Noah-MP defaults to a photosynthesis-coupled Ball-Berry scheme (Ball et al., 1987) in which stomatal conductance responds directly to CO_2 concentration. In fact, the radiative transfer is handled differently as well: CLSM interpolates surface albedo from pre-tabulated, offline-derived two-stream coefficients rescaled to MODIS climatology, while Noah-MP solves the two-stream radiative transfer equations at every time step, explicitly separating sunlit and shaded canopy fractions that feed back into stomatal conductance. All these factors differently interact with the evaporation processes, leading to differences in their ET - water level distribution. However, the overall better agreement between the Noah-MP peatland results with observations evident from the reduced errors and bias, implies a better representation of peatland microtopography in Noah-MP compared to the relatively simplified structure of that in PEATCLSM.

https://doi.org/10.5194/egusphere-2026-5287
Preprint. Discussion started: 28 October 2026
© Author(s) 2026. CC BY 4.0 License.

7.4 Limitations and sources of uncertainty

Certain aspects of this modeling framework remain unexplored due to scarce in-situ observations in the study region. For example, the scope of validating soil moisture and ET remains limited due to the lack of in-situ stations and flux towers in the region. Despite these challenges, the improved performance of the peatland module in Noah-MP with CHIRPS precipitation has been confirmed through a robust validation of water level datasets collected from 20 well locations (Fig. 10). Because all the peatland-related model changes done in the code (e.g., runoff generation, evapotranspiration stress, and storage dynamics) are explicitly dependent on water level dynamics, this validation gives some confidence that the runoff and ET responses, which depend on the same variable, are also better represented, although this remains unverified due to lack of in-situ data.

One simplification of the current peatland implementation concerns the treatment of evaporation under waterlogged conditions. The evaporation from the ponded surface is not accounted separately, and the evaporation for peat grid cells is still computed with the default Noah-MP resistance-based bare-soil formulation. This may introduce a low bias in simulated evapotranspiration during periods of surface inundation. However, we expect this bias to be of secondary importance for the Cuvette Centrale application presented here because, in our scheme, the flooding does not create a large open water surface, but rather a ponding water table that stays below the forest and understory vegetation in the Cuvette Centrale region. Under closed-canopy tropical forest, surface evaporation (whether from soil or standing water) is a minor component of total evapotranspiration relative to canopy transpiration, which dominates the water balance in these systems. We therefore consider the net effect of this simplification on grid-integrated ET to be limited in the present application.

The TWSA changes in the model have been estimated relative to GRACE TWS anomalies, accounting for the proxy surface water storage signal derived from altimetry-based DAHITI water level data and the MERIT Hydro-based surface water extent network. This approach allows us to explicitly assess the degree of SWSA contributions to the peatland water storage. However, there are uncertainties in the datasets and the model-data fusion approach may incorporate those uncertainties in this analysis. This can be avoided by employing a coupled LSM-hydrodynamic model system over the Congo peatland region (Apers et al., 2026; Getirana et al., 2021). This analysis provides insight into the limitations of uncoupled land surface modeling frameworks in exploring the river influence in peatland-dominated basins. In fact, evaluation of TWSA from the different model configurations with GRACE at this scale show marginal differences among their respective statistics. The reason behind such performance is the presence of mixed signal from both peat and non-peat, and changing the dynamics of a part of the system may not automatically lead to an improvement in the mixed system. It depends on the errors of the other unchanged part of the system as well.

Interestingly, with the same forcing input (MERRA-2), PEATCLSM shows overall improved domain average statistics of TWSA than Noah-MP with the peat module. On the contrary, the Noah-MP peatland module showed consistently improved water level estimates over the peat areas than PEATCLSM based on in-situ evaluation (Fig. 10). This contradictory behavior can be attributed to the possibility of CLSM performing better over non-peat pixels/ mineral soil than Noah-MP. NoahMP SIMTOP scheme does not account for the prognostic aquifer storage over non-peat areas like how the TOPMODEL scheme of CLSM does. However, the SIMGM approach with an optimized topographic index parameter set could enhance the NoahMP

https://doi.org/10.5194/egusphere-2026-5287
Preprint. Discussion started: 28 October 2026
© Author(s) 2026. CC BY 4.0 License.

model performance over non-peat grid cells to be more comparable with CLSM over non-peat areas, which is currently out of scope for this paper.

Despite these challenges, the study provides a broader picture of the applicability and performance of the newly introduced peatland module of Noah-MP over the complex hydrological regimes like Congo peatlands.

8 Conclusions

This study described the implementation of a peatland scheme within Noah-MP v5.0 and presented a comprehensive spatiotemporal analysis of the model performance in capturing the hydrological dynamics in the Cuvette Centrale peatland complex, in comparison with the default TOPMODEL scheme of Noah-MP and the established PEATCLSM modules in NASA's Catchment Land Surface Model (Apers et al., 2026) optimized for the same domain. The performance of this peatland module was evaluated with in-situ water level data and GRACE TWSA observations after simulating with two different precipitation inputs (MERRA-2 and CHIRPS). The impact of these modular changes was systematically analyzed by performing four test experiments based on four possible model-forcing combinations ($\text{NoahMP}_{\text{Peat=0,MER}}$, $\text{NoahMP}_{\text{Peat=0,CH}}$, $\text{NoahMP}_{\text{Peat=1,MER}}$ and $\text{NoahMP}_{\text{Peat=1,CH}}$), keeping PEATCLSM forced with MERRA-2 ($\text{PEATCLSM}_{\text{MER}}$) as reference for comparison. The key findings from the study are summarized as follows:

1. Evaluation against in-situ data demonstrates that the newly introduced peatland scheme into Noah-MPv5.0 with improved microtopographic representation better captures the peatland water level dynamics compared to the default Noah-MP configuration as well as the established PEATCLSM, enabling realistic near-surface water level estimates including the emergence of above-ground water levels (ponding in hollows). The coupled internal processes behave consistently as expected: soil moisture tracks the water level and stays persistently wet, the peatland-specific runoff scheme (with Hortonian runoff suppressed) shifts the system to a saturation-controlled regime, and a new water-level-constrained transpiration option reduces ET due to waterlogged conditions.

2. Additional evaluation against GRACE-derived total water storage anomalies indicates all the model configurations capture a similar seasonal cycle of total water storage dynamics with slightly better agreement relative to the default setup when the peatland module is forced with CHIRPS precipitation. Furthermore, accounting for the surface water storage component (rivers and lakes; not represented by Noah-MP alone) slightly improves the correlation and reduces the RMSE between Noah-MP and GRACE TWSA across all model configurations. Hence, the impact of correction accounting surface water storage contribution along with better precipitation input is more evident here than that of the peatland physics, indicating the need for better quantification of the surface water contribution from the surrounding Congo River network and lakes to peatland water storage dynamics in the Cuvette Centrale region.

3. The peat-enabled Noah-MP configuration shows performance improvements throughout most of the analysis especially when forced with CHIRPS precipitation, which is consistent with the findings of earlier studies, reporting CHIRPS as

https://doi.org/10.5194/egusphere-2026-5287
Preprint. Discussion started: 28 October 2026
© Author(s) 2026. CC BY 4.0 License.

more appropriate precipitation forcing for this region. This highlights the sensitivity of peatland hydrology to precipitation forcing and underscores the importance of accurate forcing input data.

The purpose of this study was to enhance the applicability of Noah-MP LSM to peat-dominated landscapes. However, certain modeling aspects are yet to be explored in terms of capturing better water storage dynamics and contribution of river water fluctuation on the peatland inundation. The findings of this study underscore the importance of incorporating river water storage simulation so that the current model setup can better account for TWSA magnitude and variability. Therefore, accurately reproducing GRACE signals requires an integrated modeling framework that includes land surface processes coupled with river routing and floodplain storage accumulation scheme. The water levels in the Congo peatland are likely influenced by fluctuations in the surrounding Congo River stage (Apers et al., 2026; Biddulph et al., 2021; Marthews et al., 2022), but the quantification of this influence has not yet been explored. As a future direction, implementing a fully two-way coupled land–river routing system within LIS/Noah-MP would enable dynamic exchange between river and peatland water storage and the contribution of the Congo River in the peatland flooding. Such developments would provide a more physically consistent representation of basin-scale peatland hydrology and improve the simulation of water storage and fluxes in the Congo Basin.

Code and data availability. The LIS/Noah-MPv5.0 model code with peatland-specific changes, produced and used in this study, is available at https://doi.org/10.5281/zenodo.22029413 (Chakraborty et al., 2026a). The LIS/Noah-MPv5.0 peat simulation outputs are available at the Zenodo data repository: https://doi.org/10.5281/zenodo.21396257 (Chakraborty et al., 2026b). The meteorological forcings for MERRA-2 are downloaded from https://disc.gsfc.nasa.gov/datasets?project=MERRA-2 and CHIRPS precipitation data is downloaded from https://data.chc.ucsb.edu/products/CHIRPS-2.0/. In-situ water level data used for evaluation are available at the sources indicated in Table C1. The majority of in-situ datasets are collected from https://congopeat.net/data/, published based on peer-reviewed literature (Dargie et al., 2017; Apers et al., 2026), and the rest of the datasets are provided by other co-authors and collaborators. The availability of dataset for one well location (Mai-Ndombe) is subject to an embargo associated with ongoing, unpublished PhD research by a collaborating co-author; these data have been made available in confidence to the editor and reviewers for the purposes of peer review, and will be made publicly available upon completion of that thesis work. The DAHITI dataset is accessible through https://dahiti.dgfi.tum.de/en/ and the MERIT Hydro dataset is taken from https://zenodo.org/records/4301616

https://doi.org/10.5194/egusphere-2026-5287
Preprint. Discussion started: 28 October 2026
© Author(s) 2026. CC BY 4.0 License.

Appendix A: Noah-MP Model configuration with Peatland module within LIS

Table A1. Noah-MP physics options used in this study along with the new peatland physics option

Noah-MP Physics	Option	Description
dynamic vegetation option	7	off (use input Leaf Area Index; use VegFrac = VegFracGreen from input)
canopy stomatal resistance option	1	Ball–Berry scheme (Ball et al., 1987; Bonan, 1996)
soil moisture factor for stomatal resistance option	1*	Noah (soil moisture) (Ek et al., 2003)
surface runoff option	2	TOPMODEL with an equilibrium water table (Niu et al., 2005)
subsurface runoff and groundwater option	2*	same as surface runoff option (recommended default)
peatland physics option	**1**	**Run peatland processes (New)**
surface layer drag coefficient option	1	Monin–Obukhov (M–O) Similarity Theory (Brutsaert, 1982)
supercooled liquid water option	1	No iteration (Niu and Yang, 2006)
canopy radiative transfer option	3	two-stream applied to vegetated fraction (gap = 1 - VegFrac) (Dickinson, 1983; Sellers, 1985)
snow surface albedo option	1	BATS snow albedo (Dickinson et al., 1993)
rain-snow partition option	1	Jordan scheme (Jordan, 1991)
snow thermal conductivity option	1	Stieglitz scheme (Yen, 1965)
lower boundary of soil temperature option	2	Temperature at bottom (8 m) read from file (original Noah) (Ek et al., 2003)
snow/soil temperature time scheme option	1	semi-implicit; flux top boundary condition (Niu et al., 2011)
soil configuration option	1	use input dominant soil texture
tile drainage option	0	No tile drainage
urban physics option	0	No urban physics

*For grid cells where the peatland physics option is active (soil texture class 17), the model internally overrides these two options at runtime to `OptRunoffSubsurface = 9` (Ivanov's transmissivity-decay scheme, Eq. 12–13) and `OptSoilWaterTranspiration = 4` (the peatland drought/waterlogging stress functions, Eq. 14–16), regardless of the values listed here. The values shown (2 and 1, respectively) are the model defaults and apply only to non-peat grid cells.

https://doi.org/10.5194/egusphere-2026-5287
Preprint. Discussion started: 28 October 2026
© Author(s) 2026. CC BY 4.0 License.

Appendix B: Numerical solution of the peatland soil-water balance

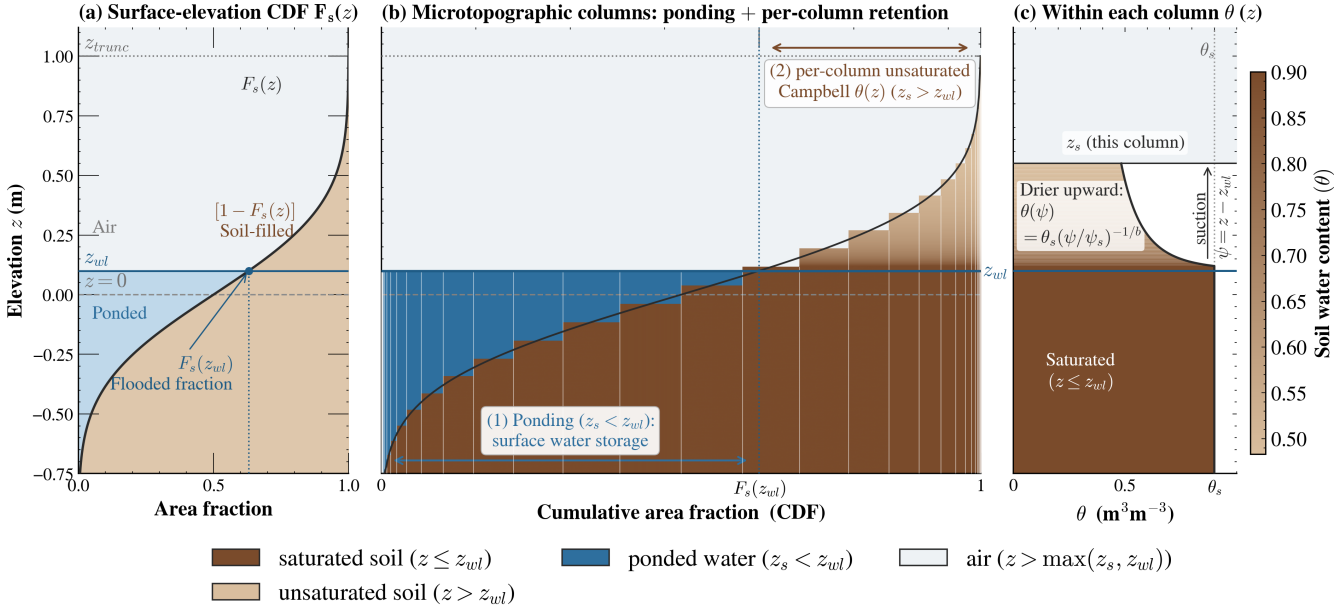


Figure B1. Subgrid microtopographic representation of a peatland grid cell (schematic, after Dettmann and Bechtold 2016; cf. Eq. 4). Local surface elevations z_s vary about the mean surface ($z = 0$, positive upward), truncated at the hummock top z_{trunc}, with a single grid-cell water level z_{wl}. (a) Surface-elevation CDF $F_s(z)$, the areal fraction with $z_s < z$; its complement $[1 - F_s(z)]$ (right of the curve) is the soil-filled fraction, and $F_s(z_{\mathrm{wl}})$ (marker) is the flooded area fraction. (b) The distribution discretized into the model's Gauss–Legendre columns, ordered by elevation with width proportional to quadrature weight so that cumulative width reproduces the CDF. Two effects require resolving the microtopography: *(1)* flooded columns ($z_s < z_{\mathrm{wl}}$) store ponded surface water, and *(2)* emergent columns ($z_s > z_{\mathrm{wl}}$) each carry an unsaturated soil column with its own retention; color shows volumetric water content θ (color bar). (c) Within-column profile $\theta(z)$: saturated below z_{wl}, and above it $\theta = \theta_s\,(\psi/\psi_s)^{-1/b}$ with suction $\psi = z - z_{\mathrm{wl}}$, air-entry head ψ_s and Campbell exponent b. Color key: saturated soil ($z \le z_{\mathrm{wl}}$), unsaturated soil ($z > z_{\mathrm{wl}}$), ponded water ($z_s < z_{\mathrm{wl}}$), air ($z > \max(z_s, z_{\mathrm{wl}})$). Elevation spread and retention parameters are illustrative.

The microtopographic storage relations of Sect. 3.2.1 are evaluated at every soil-water timestep in `SoilWaterMainMod`, supported by two dedicated modules: `PeatMicroTopoMod`, which provides the subgrid elevation distribution, the storage integrals, and the specific-yield decomposition, and `MicroTopoCorrectionMod`, which couples these to the Noah-MP water-level and soil state. At the start of each timestep the flooded fraction F_{ponded} and the soil-flux fraction f_{soil} are diagnosed from the current water level, and the incoming surface flux I_{in} is split into a soil component $I_{\mathrm{soil}} = f_{\mathrm{soil}} I_{\mathrm{in}}$ and a ponding component $I_{\mathrm{surf}} = (1 - f_{\mathrm{soil}}) I_{\mathrm{in}}$.

Shallow water levels (equilibrium regime): For water levels within 0.5 m of the surface the combined soil and surface storage,

$$S_{\mathrm{tot}}(z_{\mathrm{wl}}) = S_{\mathrm{soil}}(z_{\mathrm{wl}}) + S_{\mathrm{surf}}(z_{\mathrm{wl}}), \tag{B1}$$

https://doi.org/10.5194/egusphere-2026-5287
Preprint. Discussion started: 28 October 2026
© Author(s) 2026. CC BY 4.0 License.

is updated over one timestep as

$$S_{\mathrm{tot}}^{t+\Delta t} = S_{\mathrm{tot}}^{t} + (I_{\mathrm{soil}} + I_{\mathrm{surf}})\,\Delta t - E\,\Delta t - T\,\Delta t - Q_{\mathrm{sub}}\,\Delta t, \tag{B2}$$

where E, T, and Q_{sub} are evaporation, transpiration, and subsurface runoff. The updated water level is obtained by inverting $S_{\mathrm{tot}}(z_{\mathrm{wl}}^{t+\Delta t}) = S_{\mathrm{tot}}^{t+\Delta t}$, and the surface-ponding change follows consistently as $\Delta S_{\mathrm{surf}} = S_{\mathrm{surf}}(z_{\mathrm{wl}}^{t+\Delta t}) - S_{\mathrm{surf}}(z_{\mathrm{wl}}^{t})$.

Deeper water levels (Richards regime): For deeper water levels the one-dimensional pressure-head Richards solver of `SoilWaterDiffusionRichardsMod` is used (Eq. 8). Only the soil-domain fraction of the surface flux and sink terms is imposed on the column,

$$I_{\mathrm{soil}} = f_{\mathrm{soil}} I, \quad E_{\mathrm{soil}} = f_{\mathrm{soil}} E, \quad T_{\mathrm{soil}} = f_{\mathrm{soil}} T, \quad Q_{\mathrm{sub,soil}} = f_{\mathrm{soil}} Q_{\mathrm{sub}}, \tag{B3}$$

with the complementary fraction $(1 - f_{\mathrm{soil}})$ retained in the small remaining surface-ponding store; the evaporation, transpiration, and subsurface-runoff sinks are drawn only from the hydraulically active (unsaturated) layers above the water level. Before the update, the layer-mean soil moisture is mapped to an equivalent pressure-head anomaly relative to the hydrostatic microtopographic equilibrium; after the update, the soil-water change is transferred back to the microtopographic framework while conserving storage,

$$S_{\mathrm{soil}}^{*} = \sum_{i} \left[\theta_i^{t} + \left(\theta_{i,\mathrm{R}}^{t+\Delta t} - \theta_{i,\mathrm{R}}^{t}\right)\right] \Delta z_i, \tag{B4}$$

where θ_i^t is the original microtopography-aware layer moisture, $\theta_{i,\mathrm{R}}^t$ and $\theta_{i,\mathrm{R}}^{t+\Delta t}$ are the equivalent one-dimensional values before and after the Richards update, and Δz_i is the layer thickness. The final water level is then found by solving $S_{\mathrm{soil}}(z_{\mathrm{wl}}^{t+\Delta t}) = S_{\mathrm{soil}}^{*}$, a bisection on the microtopography-averaged storage.

Saturated layers and bottom boundary: Fully saturated layers below the diagnosed water level are decoupled from the active Richards domain, and no free drainage is permitted through the bottom of the peat column,

$$Q_{\mathrm{bot}} = 0, \tag{B5}$$

so that water added to the saturated profile raises the water level or contributes to ponding rather than being lost as artificial bottom drainage. If the diagnosed water level falls below the modeled soil column, it is capped at the column bottom and the profile reset to equilibrium there; the resulting change in column water storage is balanced against the subsurface-runoff flux to conserve mass. Together these steps keep the water level, flooded fraction, soil-moisture profile, and surface ponding mutually consistent with the subgrid hummock–hollow distribution throughout the timestep.

https://doi.org/10.5194/egusphere-2026-5287
Preprint. Discussion started: 28 October 2026
© Author(s) 2026. CC BY 4.0 License.

Appendix C: Overview of the in-situ data sites

Table C1. List of in-situ well locations:

No.	Well ID	Lon (°)	Lat (°)	Data availability	Source
1	Bondonki-SPT4	17.0285	0.8549	Apr 2013 – May 2014	Dargie et al. (2017)
2	Bondonki-SPT5	17.0196	0.8552	Apr 2013 – May 2014	Dargie et al. (2017)
3	Bondonki-SPT6	17.0105	0.8555	Apr 2013 – May 2014	Dargie et al. (2017)
4	Bondzale-SPT3	17.9863	1.9083	Mar 2013 – May 2014	Dargie et al. (2017)
5	Bondzale-SPT4	17.9777	1.9070	Mar 2013 – May 2014	Dargie et al. (2017)
6	Bondzale-SPT6	17.9595	1.9041	Mar 2013 – May 2014	Dargie et al. (2017)
7	Ekolongouma-EKG2	17.8466	1.1915	Mar 2019 – Mar 2021	Dargie et al. (2017)
8	Ekolongouma-EKG3	17.8315	1.1883	Mar 2019 – Mar 2021	Dargie et al. (2017)
9	Ekolongouma-SPT0	17.7963	1.1808	Feb 2013 – Mar 2015, Mar 2017 – Sep 2018	Dargie et al. (2017)
10	Ekolongouma-SPT2	17.8139	1.1846	Apr 2014 – Mar 2015, Mar 2017 – Sep 2018	Dargie et al. (2017)
11	Ekolongouma-SPT4	17.8315	1.1879	Feb 2013 – Apr 2014, Mar 2017 – Sep 2018	Dargie et al. (2017)
12	Ekolongouma-SPT5	17.8402	1.1899	Feb 2013 – Mar 2015, Mar 2017 – Sep 2018	Dargie et al. (2017)
13	Itanga-SPT3	17.4609	1.2085	Mar 2013 – Apr 2015, Feb 2017 – Aug 2018	Dargie et al. (2017)
14	Itanga-SPT5	17.4870	1.2151	Mar 2013 – Apr 2015, Feb 2017 – Aug 2018	Dargie et al. (2017)
15	Itanga-SPT6	17.4782	1.2129	Mar 2013 – Apr 2015, Feb 2017 – Aug 2018	Dargie et al. (2017)
16	Lokolama-5.1	18.2007	-0.3032	Feb 2018 – Dec 2019	Crezee (2022)
17	Lokolama-5.3	18.1871	-0.3150	Feb 2018 – Dec 2019	Crezee (2022)
18	Lokolama-5.4	18.1803	-0.3209	Feb 2018 – Dec 2019	Crezee (2022)
19	Ikelemba-5	18.8276	0.2834	Mar 2018 – Nov 2019	Crezee (2022)
20	Mai-Ndombe	18.3812	-1.8812	Aug 2024 – Jul 2025	Unpublished

https://doi.org/10.5194/egusphere-2026-5287
Preprint. Discussion started: 28 October 2026
© Author(s) 2026. CC BY 4.0 License.

Table C2. Performance metrics (R, RMSE, Bias, ubRMSE) for different model configurations at each dip well. Here the values of RMSE, Bias, and ubRMSE are in 'm'.

Well ID	$\mathbf{NoahMP_{Peat=0,MER}}$				$\mathbf{NoahMP_{Peat=0,CH}}$				$\mathbf{NoahMP_{Peat=1,MER}}$				$\mathbf{NoahMP_{Peat=1,CH}}$				$\mathbf{PEATCLSM_{MER}}$			
	R	**RMSE**	**Bias**	**ubRMSE**	**R**	**RMSE**	**Bias**	**ubRMSE**	**R**	**RMSE**	**Bias**	**ubRMSE**	**R**	**RMSE**	**Bias**	**ubRMSE**	**R**	**RMSE**	**Bias**	**ubRMSE**
Bondonki-SPT4	0.68	1.59	-1.52	0.46	0.78	1.37	-1.33	0.31	0.72	0.11	0.03	0.11	0.80	0.13	0.10	0.09	0.87	0.36	-0.31	0.17
Bondonki-SPT5	0.04	1.78	-1.75	0.34	0.43	1.51	-1.49	0.25	0.35	0.11	0.00	0.11	0.64	0.11	0.08	0.07	0.38	0.46	-0.44	0.15
Bondonki-SPT6	0.25	1.78	-1.75	0.33	0.57	1.52	-1.50	0.23	0.48	0.10	-0.01	0.10	0.71	0.10	0.08	0.06	0.48	0.46	-0.44	0.14
Bondzale-SPT3	0.27	1.79	-1.59	0.83	0.53	1.57	-1.48	0.51	0.25	0.27	-0.07	0.26	0.55	0.14	-0.01	0.14	0.40	0.37	-0.23	0.30
Bondzale-SPT4	0.11	1.75	-1.53	0.85	0.40	1.52	-1.42	0.53	0.09	0.28	-0.01	0.28	0.41	0.17	0.05	0.16	0.25	0.36	-0.17	0.32
Bondzale-SPT6	-0.12	1.78	-1.53	0.93	0.17	1.53	-1.42	0.59	-0.12	0.39	-0.01	0.39	0.23	0.27	0.05	0.27	0.06	0.43	-0.16	0.40
Ekolongouma-EKG2	0.60	1.83	-1.72	0.63	0.68	1.44	-1.38	0.43	0.55	0.24	-0.08	0.22	0.63	0.18	0.05	0.18	0.56	0.44	-0.37	0.25
Ekolongouma-EKG3	0.62	1.79	-1.68	0.62	0.70	1.40	-1.34	0.42	0.58	0.22	-0.04	0.21	0.66	0.19	0.09	0.17	0.54	0.41	-0.32	0.26
Ekolongouma-SPT0	0.12	1.57	-1.40	0.70	0.29	1.35	-1.27	0.45	-0.00	0.27	-0.02	0.26	0.28	0.18	0.04	0.17	0.03	0.39	-0.21	0.34
Ekolongouma-SPT2	0.37	1.48	-1.32	0.67	0.50	1.26	-1.18	0.45	0.24	0.22	0.03	0.22	0.51	0.16	0.10	0.12	0.35	0.32	-0.14	0.29
Ekolongouma-SPT4	0.44	1.39	-1.26	0.59	0.44	1.30	-1.23	0.43	0.42	0.16	0.03	0.16	0.48	0.14	0.05	0.13	0.52	0.25	-0.13	0.21
Ekolongouma-SPT5	0.40	1.48	-1.33	0.65	0.46	1.27	-1.20	0.42	0.31	0.22	0.04	0.21	0.48	0.18	0.11	0.15	0.38	0.31	-0.14	0.28
Itanga-SPT3	0.38	1.49	-1.34	0.65	0.40	1.29	-1.20	0.46	0.35	0.23	0.06	0.23	0.47	0.22	0.12	0.18	0.46	0.31	-0.15	0.27
Itanga-SPT5	0.44	1.56	-1.42	0.65	0.44	1.35	-1.27	0.46	0.40	0.21	-0.01	0.21	0.51	0.16	0.05	0.15	0.51	0.34	-0.22	0.26
Itanga-SPT6	0.52	1.50	-1.37	0.63	0.48	1.31	-1.23	0.45	0.50	0.18	0.03	0.18	0.54	0.17	0.10	0.14	0.59	0.30	-0.18	0.24
Mai-Ndombe	0.84	1.84	-1.75	0.57	0.95	1.71	-1.62	0.54	0.88	0.32	-0.28	0.15	0.92	0.28	-0.23	0.15	0.74	0.63	-0.60	0.21
Lokolama-5.1	0.45	1.07	-1.02	0.32	0.45	1.33	-1.26	0.41	0.46	0.13	0.09	0.08	0.34	0.11	0.04	0.11	0.31	0.16	-0.05	0.15
Lokolama-5.3	0.54	1.05	-1.00	0.30	0.41	1.31	-1.25	0.41	0.54	0.12	0.10	0.07	0.28	0.11	0.05	0.10	0.34	0.15	-0.04	0.15
Lokolama-5.4	0.52	1.05	-1.00	0.30	0.36	1.32	-1.25	0.42	0.52	0.13	0.10	0.07	0.24	0.12	0.04	0.11	0.29	0.16	-0.04	0.15
Ikelemba-5	0.62	0.86	-0.84	0.21	0.58	0.86	-0.84	0.18	0.64	0.28	0.27	0.09	0.60	0.29	0.28	0.10	0.49	0.22	0.18	0.13

https://doi.org/10.5194/egusphere-2026-5287
Preprint. Discussion started: 28 October 2026
© Author(s) 2026. CC BY 4.0 License.

Author contributions. MB, AC, CH, DMM, and SVK proposed the research idea and explored the possibilities and future scopes of the model development. AC and MB contributed to the development of peatland-specific modules within the Noah-MP source code with the help of CH. AC performed model simulations and evaluations with contributions from PW and GDL, who provided hydrological insights of the implementation.BC,LN and RMT provided additional in-situ data for model evaluation. AC drafted the manuscript with the inputs from MB, PW, GDL, DMM, SVK, AG, CH, LN, BC, RMT.

Competing interests. C. He is serving on the journal Editorial Board of Geoscientific Model Development. Other authors declare that they have no known competing financial interests or personal relationships that could have appeared to influence the work reported in this paper.

Acknowledgements. The authors would like to acknowledge the Vlaams Supercomputer Centrum (VSC) for providing computational and storage resources, funded by FWO and the Flemish Government (incl. Storage4Climate collaborative grant). Other internal technical support regarding the model and HPC setup was offered by Samuel Corveleyn. The authors gratefully acknowledge financial support for this work through grants from the STEREO IV project EO4PEAT (SR/00/414) funded by the Belgian Science Policy (BELSPO). The authors gratefully acknowledge Greta C. Dargie for providing the in-situ water level datasets for the locations in the Republic of Congo.

https://doi.org/10.5194/egusphere-2026-5287
Preprint. Discussion started: 28 October 2026
© Author(s) 2026. CC BY 4.0 License.

References

Alsdorf, D., Beighley, E., Laraque, A., Lee, H., Tshimanga, R., O'Loughlin, F., Mahé, G., Dinga, B., Moukandi, G., and Spencer, R. G. M.: Opportunities for Hydrologic Research in the Congo Basin, Reviews of Geophysics, 54, 378–409, https://doi.org/10.1002/2016RG000517, 2016.

Apers, S., De Lannoy, G. J. M., Baird, A. J., Cobb, A. R., Dargie, G. C., del Aguila Pasquel, J., Gruber, A., Hastie, A., Hidayat, H., Hirano, T., Hoyt, A. M., Jovani-Sancho, A. J., Katimon, A., Kurnain, A., Koster, R. D., Lampela, M., Mahanama, S. P. P., Melling, L., Page, S. E., Reichle, R. H., Taufik, M., Vanderborght, J., and Bechtold, M.: Tropical Peatland Hydrology Simulated With a Global Land Surface Model, Journal of Advances in Modeling Earth Systems, 14, e2021MS002 784, https://doi.org/10.1029/2021MS002784, 2022.

Apers, S., Cobb, A. R., De Lannoy, G. J. M., and Bechtold, M.: Characterising Tropical Peatland Hydrological Response With Satellite-Based Rainfall: A Case Study in Brunei, Hydrological Processes, 39, e70 209, https://doi.org/10.1002/hyp.70209, 2025.

Apers, S., De Lannoy, G. J. M., Bocko, Y. E., Cobb, A. R., Dargie, G., Davenport, I., Reichle, R. H., Mampouya Wenina, Y. E., Mbemba, M., and Bechtold, M.: Insights into the hydrology of the Cuvette Centrale peatlands through SMOS L-band data assimilation into an enhanced land surface model, ESS Open Archive, 2026, https://doi.org/10.22541/essoar.15004681/v1, preprint, submitted to Journal of Advances in Modeling Earth Systems (JAMES), 2026.

Arsenault, K. R., Kumar, S. V., Geiger, J. V., Wang, S., Kemp, E., Mocko, D. M., Beaudoing, H. K., Getirana, A., Navari, M., Li, B., Jacob, J., Wegiel, J., and Peters-Lidard, C. D.: The Land surface Data Toolkit (LDT v7. 2)–a data fusion environment for land data assimilation systems, Geoscientific Model Development, 11, 3605–3621, 2018.

Baird, A. J.: Field Estimation of Macropore Functioning and Surface Hydraulic Conductivity in a Fen Peat, Hydrological Processes, 11, 287–295, https://doi.org/10.1002/(SICI)1099-1085(19970315)11:3<287::AID-HYP443>3.0.CO;2-L, 1997.

Baird, A. J., Low, R., Young, D., Swindles, G. T., Lopez, O. R., and Page, S.: High Permeability Explains the Vulnerability of the Carbon Store in Drained Tropical Peatlands, Geophysical Research Letters, 44, 1333–1339, https://doi.org/10.1002/2016GL072245, 2017.

Ball, J. T., Woodrow, I. E., and Berry, J. A.: A model predicting stomatal conductance and its contribution to the control of photosynthesis under different environmental conditions, in: Progress in Photosynthesis Research, edited by Biggins, J., pp. 221–224, Springer, Dordrecht, https://doi.org/10.1007/978-94-017-0519-6_48, 1987.

Bechtold, M., De Lannoy, G. J. M., Koster, R. D., Reichle, R. H., Mahanama, S. P., Bleuten, W., Bourgault, M. A., Brümmer, C., Burdun, I., Desai, A. R., Devito, K., Grünwald, T., Grygoruk, M., Humphreys, E. R., Klatt, J., Kurbatova, J., Lohila, A., Munir, T. M., Nilsson, M. B., Price, J. S., Röhl, M., Schneider, A., and Tiemeyer, B.: PEAT-CLSM: A Specific Treatment of Peatland Hydrology in the NASA Catchment Land Surface Model, Journal of Advances in Modeling Earth Systems, 11, 2130–2162, https://doi.org/10.1029/2018MS001574, 2019.

Biddulph, G. E., Bocko, Y. E., Bola, P., Crezee, B., Dargie, G. C., Emba, O., Georgiou, S., Girkin, N., Hawthorne, D., Jovani-Sancho, J., Kanyama T., J., Mampouya, W. E., Mbemba, M., Sciumbata, M., and Tyrrell, G.: Current Knowledge on the Cuvette Centrale Peatland Complex and Future Research Directions, Bois for. trop., 350, 3–14, https://doi.org/10.19182/bft2021.350.a36288, 2021.

Biddulph, G. E., Bocko, Y. E., Bola, P., Crezee, B., Dargie, G., Emba, O., Georgiou, S., Girkin, N., Hawthorne, D., Sancho, J. J., T, J. K., Mampouya, W. E., Mbemba, M., Sciumbata, M., and Tyrrell, G.: Connaissances actuelles et orientations futures des recherches sur le complexe de tourbières de la Cuvette centrale du Congo, BOIS & FORETS DES TROPIQUES, 355, 73–86, https://doi.org/10.19182/bft2023.355.a37152, 2023.

https://doi.org/10.5194/egusphere-2026-5287
Preprint. Discussion started: 28 October 2026
© Author(s) 2026. CC BY 4.0 License.



Bonan, G. B.: A Land Surface Model (LSM Version 1.0) for Ecological, Hydrological, and Atmospheric Studies: Technical Description and User's Guide, NCAR Technical Note NCAR/TN-417+STR, National Center for Atmospheric Research, Boulder, CO, https://doi.org/10.5065/D6DF6P5X, 1996.

Brutsaert, W.: Evaporation into the Atmosphere: Theory, History and Applications, D. Reidel Publishing Company, Dordrecht, Holland, 1982.

Busker, T., de Roo, A., Gelati, E., Schwatke, C., Adamovic, M., Bisselink, B., Pekel, J.-F., and Cottam, A.: A global lake and reservoir volume analysis using a surface water dataset and satellite altimetry, Hydrology and Earth System Sciences, 23, 669–690, https://doi.org/10.5194/hess-23-669-2019, 2019.

Campbell, G. S.: A Simple Method for Determining Unsaturated Conductivity from Moisture Retention Data, Soil Science, 117, 311, 1974.

Chakraborty, A., Willems, P., De Lannoy, G. J. M., Mocko, D. M., Kumar, S. V., He, C., Getirana, A., and Bechtold, M.: LISF/Noah-MP version 5.0 coupled source code with peatland specific modules, Figure, https://doi.org/10.5281/zenodo.22029413, 2026a.

Chakraborty, A., Willems, P., De Lannoy, G. J. M., Mocko, D. M., Kumar, S. V., He, C., Getirana, A., and Bechtold, M.: LIS/Noah-MPv5 PEAT simulated outputs supporting: "Peatland hydrology in Noah-MP land surface model v5.0: parameterization and evaluation over the Congo peatlands", Dataset, https://doi.org/10.5281/zenodo.21396257, 2026b.

Chen, J., Liao, J., Gao, L., and Wang, X.: A dataset for lake level changes in the Tibetan Plateau (2002/2010 to 2021) using multi-altimeter data, Earth System Science Data, 17, 4235–4252, https://doi.org/10.5194/essd-17-4235-2025, 2025.

Clapp, R. B. and Hornberger, G. M.: Empirical equations for some soil hydraulic properties, Water Resources Research, 14, 601–604, https://doi.org/10.1029/WR014i004p00601, 1978.

Cobb, A. R., Hoyt, A. M., Gandois, L., Eri, J., Dommain, R., Abu Salim, K., Kai, F. M., Haji Su'ut, N. S., and Harvey, C. F.: How Temporal Patterns in Rainfall Determine the Geomorphology and Carbon Fluxes of Tropical Peatlands, Proceedings of the National Academy of Sciences, 114, E5187–E5196, https://doi.org/10.1073/pnas.1701090114, 2017.

Cosby, B. J., Hornberger, G. M., Clapp, R. B., and Ginn, T. R.: A statistical exploration of the relationships of soil moisture characteristics to the physical properties of soils, Water Resources Research, 20, 682–690, https://doi.org/10.1029/WR020i006p00682, 1984.

Crezee, B., Dargie, G. C., Ewango, C. E. N., Mitchard, E. T. A., Emba B., O., Kanyama T., J., Bola, P., Ndjango, J.-B. N., Girkin, N. T., Bocko, Y. E., Ifo, S. A., Hubau, W., Seidensticker, D., Batumike, R., Imani, G., Cuní-Sanchez, A., Kiahtipes, C. A., Lebamba, J., Wotzka, H.-P., Bean, H., Baker, T. R., Baird, A. J., Boom, A., Morris, P. J., Page, S. E., Lawson, I. T., and Lewis, S. L.: Mapping Peat Thickness and Carbon Stocks of the Central Congo Basin Using Field Data, Nat. Geosci., 15, 639–644, https://doi.org/10.1038/s41561-022-00966-7, 2022.

Crezee, B. J.: Spatial distribution, carbon stocks and diversity of peat swamp forests in the central Congo Basin, Phd thesis, University of Leeds, https://etheses.whiterose.ac.uk/id/eprint/32358/, 2022.

Dargie, G. C., Lewis, S. L., Lawson, I. T., Mitchard, E. T. A., Page, S. E., Bocko, Y. E., and Ifo, S. A.: Age, Extent and Carbon Storage of the Central Congo Basin Peatland Complex, Nature, 542, 86–90, https://doi.org/10.1038/nature21048, 2017.

Dargie, G. C., Lawson, I. T., Rayden, T. J., Miles, L., Mitchard, E. T. A., Page, S. E., Bocko, Y. E., Ifo, S. A., and Lewis, S. L.: Congo Basin Peatlands: Threats and Conservation Priorities, Mitig Adapt Strateg Glob Change, 24, 669–686, https://doi.org/10.1007/s11027-017-9774-8, 2019.

Datok, P., Fabre, C., Sauvage, S., N'kaya, G. D. M., Paris, A., Santos, V. D., Laraque, A., and Sánchez-Pérez, J.-M.: Investigating the Role of the Cuvette Centrale in the Hydrology of the Congo River Basin, in: Congo Basin Hydrology, Climate, and Biogeochemistry, chap. 14, pp. 247–273, American Geophysical Union (AGU), ISBN 978-1-119-65700-2, https://doi.org/10.1002/9781119657002.ch14, 2022.

https://doi.org/10.5194/egusphere-2026-5287
Preprint. Discussion started: 28 October 2026
© Author(s) 2026. CC BY 4.0 License.

Davenport, I. J., McNicol, I., Mitchard, E. T. A., Dargie, G., Suspense, I., Milongo, B., Bocko, Y. E., Hawthorne, D., Lawson, I., Baird, A. J., Page, S., and Lewis, S. L.: First Evidence of Peat Domes in the Congo Basin Using LiDAR from a Fixed-Wing Drone, Remote Sensing, 12, https://doi.org/10.3390/rs12142196, 2020.

Dettmann, U. and Bechtold, M.: One-Dimensional Expression to Calculate Specific Yield for Shallow Groundwater Systems with Microrelief, Hydrological Processes, 30, 334–340, https://doi.org/10.1002/hyp.10637, 2016.

Dickinson, R. E.: Land Surface Processes and Climate—Surface Albedos and Energy Balance, in: Advances in Geophysics, vol. 25, pp. 305–353, Elsevier, https://doi.org/10.1016/S0065-2687(08)60176-4, 1983.

Dickinson, R. E., Henderson-Sellers, A., Kennedy, P. J., and Wilson, M. F.: Biosphere-Atmosphere Transfer Scheme (BATS) Version 1e as Coupled to the NCAR Community Climate Model, NCAR Technical Note NCAR/TN-387+STR, National Center for Atmospheric Research, Boulder, CO, https://doi.org/10.5065/D67W6959, 1993.

Dinku, T., Funk, C., Peterson, P., Maidment, R., Tadesse, T., Gadain, H., and Ceccato, P.: Validation of the CHIRPS Satellite Rainfall Estimates over Eastern Africa, Quarterly Journal of the Royal Meteorological Society, 144, 292–312, https://doi.org/10.1002/qj.3244, 2018.

Dommain, R., Couwenberg, J., and Joosten, H.: Hydrological Self-Regulation of Domed Peatlands in South-East Asia and Consequences for Conservation and Restoration, Mires and Peat, 6, 1–17, https://doi.org/10.19189/001c.128357, 2010.

Dommain, R., Couwenberg, J., and Joosten, H.: Development and Carbon Sequestration of Tropical Peat Domes in South-East Asia: Links to Post-Glacial Sea-Level Changes and Holocene Climate Variability, Quaternary Science Reviews, 30, 999–1010, https://doi.org/10.1016/j.quascirev.2011.01.018, 2011.

Dos Santos, V., Oliveira, R., Datok, P., Sauvage, S., Paris, A., Gosset, M., and Sánchez-Pérez, J.: Evaluating the Performance of Multiple Satellite-Based Precipitation Products in the Congo River Basin Using the SWAT Model, Journal of Hydrology: Regional Studies, 42, 101 168, https://doi.org/10.1016/j.ejrh.2022.101168, 2022.

Ducharne, A., Koster, R. D., Suarez, M. J., Stieglitz, M., and Kumar, P.: A Catchment-Based Approach to Modeling Land Surface Processes in a General Circulation Model: 2. Parameter Estimation and Model Demonstration, Journal of Geophysical Research: Atmospheres, 105, 24 823–24 838, https://doi.org/10.1029/2000JD900328, 2000.

Eilander, D., van Verseveld, W., Yamazaki, D., Weerts, A., Winsemius, H. C., and Ward, P. J.: A hydrography upscaling method for scale-invariant parametrization of distributed hydrological models, Hydrology and Earth System Sciences, 25, 5287–5313, https://doi.org/10.5194/hess-25-5287-2021, 2021.

Ek, M. B., Mitchell, K. E., Lin, Y., Rogers, E., Grunmann, P., Koren, V., Gayno, G., and Tarpley, J. D.: Implementation of Noah Land Surface Model Advances in the National Centers for Environmental Prediction Operational Mesoscale Eta Model, Journal of Geophysical Research: Atmospheres, 108, https://doi.org/10.1029/2002JD003296, 2003.

Elenga, H., Schwartz, D., and Vincens, A.: Pollen Evidence of Late Quaternary Vegetation and Inferred Climate Changes in Congo, Palaeogeography, Palaeoclimatology, Palaeoecology, 109, 345–356, https://doi.org/10.1016/0031-0182(94)90184-8, 1994.

Fischer, G., Nachtergaele, F., Prieler, S., van Velthuizen, H. T., Verelst, L., and Wiberg, D.: Global Agro-ecological Zones Assessment for Agriculture (GAEZ 2008), Tech. rep., IIASA, Laxenburg, Austria and FAO, Rome, Italy, https://www.fao.org/soils-portal/data-hub/soil-maps-and-databases/harmonized-world-soil-database-v12/en/, 2008.

Friedl, M. A., McIver, D. K., Hodges, J. C. F., Zhang, X. Y., Muchoney, D., Strahler, A. H., Woodcock, C. E., Gopal, S., Schneider, A., Cooper, A., Baccini, A., Gao, F., and Schaaf, C.: Global land cover mapping from MODIS: algorithms and early results, Remote Sensing of Environment, 83, 287–302, https://doi.org/10.1016/S0034-4257(02)00078-0, 2002.

https://doi.org/10.5194/egusphere-2026-5287
Preprint. Discussion started: 28 October 2026
© Author(s) 2026. CC BY 4.0 License.

Frolking, S., Talbot, J., Jones, M. C., Treat, C. C., Kauffman, J. B., Tuittila, E.-S., and Roulet, N.: Peatlands in the Earth's 21st Century Climate System, Environ. Rev., 19, 371–396, https://doi.org/10.1139/a11-014, 2011.

Funk, C., Peterson, P., Landsfeld, M., Pedreros, D., Verdin, J., Shukla, S., Husak, G., Rowland, J., Harrison, L., Hoell, A., and Michaelsen, J.: The climate hazards infrared precipitation with stations—a new environmental record for monitoring extremes, Scientific Data, 2, 150 066, https://doi.org/10.1038/sdata.2015.66, 2015.

Garcin, Y., Schefuß, E., Dargie, G. C., Hawthorne, D., Lawson, I. T., Sebag, D., Biddulph, G. E., Crezee, B., Bocko, Y. E., Ifo, S. A., Mampouya Wenina, Y. E., Mbemba, M., Ewango, C. E. N., Emba, O., Bola, P., Kanyama Tabu, J., Tyrrell, G., Young, D. M., Gassier, G., Girkin, N. T., Vane, C. H., Adatte, T., Baird, A. J., Boom, A., Gulliver, P., Morris, P. J., Page, S. E., Sjögersten, S., and Lewis, S. L.: Hydroclimatic Vulnerability of Peat Carbon in the Central Congo Basin, Nature, 612, 277–282, https://doi.org/10.1038/s41586-022-05389-3, 2022.

Gelaro, R., McCarty, W., Suárez, M. J., Todling, R., Molod, A., Takacs, L., Randles, C. A., Darmenov, A., Bosilovich, M. G., Reichle, R., Wargan, K., Coy, L., Cullather, R., Draper, C., Akella, S., Buchard, V., Conaty, A., da Silva, A. M., Gu, W., Kim, G.-K., Koster, R., Lucchesi, R., Merkova, D., Nielsen, J. E., Partyka, G., Pawson, S., Putman, W., Rienecker, M., Schubert, S. D., Sienkiewicz, M., and Zhao, B.: The Modern-Era Retrospective Analysis for Research and Applications, Version 2 (MERRA-2), Journal of Climate, 30, 5419–5454, https://doi.org/10.1175/JCLI-D-16-0758.1, 2017.

Getirana, A., Kumar, S. V., Konapala, G., and Ndehedehe, C. E.: Impacts of Fully Coupling Land Surface and Flood Models on the Simulation of Large Wetlands' Water Dynamics: The Case of the Inner Niger Delta, Journal of Advances in Modeling Earth Systems, 13, e2021MS002 463, https://doi.org/10.1029/2021MS002463, 2021.

Guan, K., Pan, M., Li, H., Wolf, A., Wu, J., Medvigy, D., Caylor, K. K., Sheffield, J., Wood, E. F., Malhi, Y., Liang, M., Kimball, J. S., Saleska, S. R., Berry, J., Joiner, J., and Lyapustin, A. I.: Photosynthetic Seasonality of Global Tropical Forests Constrained by Hydroclimate, Nature Geoscience, 8, 284–289, https://doi.org/10.1038/ngeo2382, 2015.

Gutman, G. and Ignatov, A.: The derivation of the green vegetation fraction from NOAA/AVHRR data for use in numerical weather prediction models, International Journal of Remote Sensing, 19, 1533–1543, https://doi.org/10.1080/014311698215333, 1998.

Hastie, A., Householder, J. E., Honorio Coronado, E. N., Hidalgo Pizango, C. G., Herrera, R., Lähteenoja, O., de Jong, J., Winton, R. S., Aymard Corredor, G. A., Reyna, J., Montoya, E., Paukku, S., Mitchard, E. T. A., Åkesson, C. M., Baker, T. R., Cole, L. E. S., Córdova Oroche, C. J., Dávila, N., Águila, J. D., Draper, F. C., Fluet-Chouinard, E., Grández, J., Janovec, J. P., Reyna, D., W Tobler, M., Del Castillo Torres, D., Roucoux, K. H., Wheeler, C. E., Fernandez Piedade, M. T., Schöngart, J., Wittmann, F., van der Zon, M., and Lawson, I. T.: A New Data-Driven Map Predicts Substantial Undocumented Peatland Areas in Amazonia, Environ. Res. Lett., 19, 094 019, https://doi.org/10.1088/1748-9326/ad677b, 2024.

Hawthorne, D., Lawson, I. T., Dargie, G. C., Bocko, Y. E., Ifo, S. A., Garcin, Y., Schefuß, E., Hiles, W., Jovani-Sancho, A. J., Tyrrell, G., Biddulph, G. E., Boom, A., Chase, B. M., Gulliver, P., Page, S. E., Roucoux, K. H., Sjögersten, S., Young, D. M., and Lewis, S. L.: Genesis and Development of an Interfluvial Peatland in the Central Congo Basin since the Late Pleistocene, Quaternary Science Reviews, 305, 107 992, https://doi.org/10.1016/j.quascirev.2023.107992, 2023.

He, C., Valayamkunnath, P., Barlage, M., Chen, F., Gochis, D., Cabell, R., Schneider, T., Rasmussen, R., Niu, G.-Y., Yang, Z.-L., Niyogi, D., and Ek, M.: The Community Noah-MP Land Surface Modeling System Technical Description Version 5.0, Tech. Rep. NCAR/TN-575+STR, National Center for Atmospheric Research, https://doi.org/10.5065/ew8g-yr95, 2023a.

He, C., Valayamkunnath, P., Barlage, M., Chen, F., Gochis, D., Cabell, R., Schneider, T., Rasmussen, R., Niu, G.-Y., Yang, Z.-L., Niyogi, D., and Ek, M.: Modernizing the Open-Source Community Noah with Multi-Parameterization Options (Noah-MP) Land Surface

https://doi.org/10.5194/egusphere-2026-5287
Preprint. Discussion started: 28 October 2026
© Author(s) 2026. CC BY 4.0 License.

Model (Version 5.0) with Enhanced Modularity, Interoperability, and Applicability, Geoscientific Model Development, 16, 5131–5151, https://doi.org/10.5194/gmd-16-5131-2023, 2023b.

He, C., Lin, T.-S., Mocko, D. M., Abolafia-Rosenzweig, R., Wegiel, J. W., and Kumar, S. V.: Benchmarking and evaluating the NASA Land Information System (version 7.5.2) coupled with the refactored Noah-MP land surface model (version 5.0), Geoscientific Model Development, 18, 8439–8460, https://doi.org/10.5194/gmd-18-8439-2025, 2025.

Hirano, T., Kusin, K., Limin, S., and Osaki, M.: Evapotranspiration of Tropical Peat Swamp Forests, Global Change Biology, 21, 1914–1927, https://doi.org/10.1111/gcb.12653, 2015.

Honorio Coronado, E. N., Hastie, A., Reyna, J., Flores, G., Grández, J., Lähteenoja, O., Draper, F. C., Åkesson, C. M., Baker, T. R., Bhomia, R. K., Cole, L. E. S., Dávila, N., Del Águila, J., Del Águila, M., Del Castillo Torres, D., Lawson, I. T., Martín Brañas, M., Mitchard, E. T. A., Monteagudo, A., Phillips, O. L., Ramírez, E., Ríos, M., Ríos, S., Rodriguez, L., Roucoux, K. H., Tagle Casapia, X., Vasquez, R., Wheeler, C. E., and Montoya, M.: Intensive Field Sampling Increases the Known Extent of Carbon-Rich Amazonian Peatland Pole Forests, Environ. Res. Lett., 16, 074 048, https://doi.org/10.1088/1748-9326/ac0e65, 2021.

Ishii, Y., Koizumi, K., Fukami, H., Yamamoto, K., Takahashi, H., Limin, S. H., Kusin, K., Usup, A., and Susilo, G. E.: Groundwater in Peatland, in: Tropical Peatland Ecosystems, edited by Osaki, M. and Tsuji, N., pp. 265–279, Springer Japan, Tokyo, ISBN 978-4-431-55681-7, https://doi.org/10.1007/978-4-431-55681-7_17, 2016.

Joosten, H. and Clarke, D.: Wise Use of Mires and Peatlands: Background and Principles Including a Framework for Decision-Making, Internat. Mire Conservation Group [u.a.], Totnes, ISBN 978-951-97744-8-0, 2002.

Jordan, R. E.: A One-Dimensional Temperature Model for a Snow Cover: Technical Documentation for SNTHERM.89, CRREL Special Report 91-16, U.S. Army Cold Regions Research and Engineering Laboratory, Hanover, NH, https://hdl.handle.net/11681/11677, 1991.

Kelly, T. J., Baird, A. J., Roucoux, K. H., Baker, T. R., Honorio Coronado, E. N., Ríos, M., and Lawson, I. T.: The High Hydraulic Conductivity of Three Wooded Tropical Peat Swamps in Northeast Peru: Measurements and Implications for Hydrological Function, Hydrological Processes, 28, 3373–3387, https://doi.org/10.1002/hyp.9884, 2014.

Koster, R. D., Suarez, M. J., Ducharne, A., Stieglitz, M., and Kumar, P.: A Catchment-Based Approach to Modeling Land Surface Processes in a General Circulation Model: 1. Model Structure, Journal of Geophysical Research: Atmospheres, 105, 24 809–24 822, https://doi.org/10.1029/2000JD900327, 2000.

Kouakou, C., Paturel, J.-E., Satgé, F., Tramblay, Y., Defrance, D., and Rouché, N.: Comparison of Gridded Precipitation Estimates for Regional Hydrological Modeling in West and Central Africa, Journal of Hydrology: Regional Studies, 47, 101 409, https://doi.org/10.1016/j.ejrh.2023.101409, 2023.

Kumar, S. V., Peters-Lidard, C. D., Tian, Y., Houser, P. R., Geiger, J., Olden, S., Lighty, L., Eastman, J. L., Doty, B., Dirmeyer, P., Adams, J., Mitchell, K., Wood, E. F., and Sheffield, J.: Land information system: An interoperable framework for high resolution land surface modeling, Environmental modelling & software, 21, 1402–1415, 2006.

Kumar, S. V., Reichle, R. H., Peters-Lidard, C. D., Koster, R. D., Zhan, X., Crow, W. T., Eylander, J. B., and Houser, P. R.: A land surface data assimilation framework using the land information system: Description and applications, Advances in Water Resources, 31, 1419–1432, 2008.

Lampela, M., Jauhiainen, J., Kämäri, I., Koskinen, M., Tanhuanpää, T., Valkeapää, A., and Vasander, H.: Ground Surface Microtopography and Vegetation Patterns in a Tropical Peat Swamp Forest, CATENA, 139, 127–136, https://doi.org/10.1016/j.catena.2015.12.016, 2016.

Landerer, F. W., Flechtner, F. M., Save, H., Webb, F. H., Bandikova, T., Bertiger, W. I., Bettadpur, S. V., Byun, S. H., Dahle, C., Dobslaw, H., Fahnestock, E., Harvey, N., Kang, Z., Kruizinga, G. L. H., Loomis, B. D., McCullough, C., Murböck, M., Nagel, P., Paik, M., Pie,

https://doi.org/10.5194/egusphere-2026-5287
Preprint. Discussion started: 28 October 2026
© Author(s) 2026. CC BY 4.0 License.

N., Poole, S., Strekalov, D., Tamisiea, M. E., Wang, F., Watkins, M. M., Wen, H.-Y., Wiese, D. N., and Yuan, D.-N.: Extending the Global Mass Change Data Record: GRACE Follow-On Instrument and Science Data Performance, Geophysical Research Letters, 47, e2020GL088 306, https://doi.org/10.1029/2020GL088306, 2020.

Laraque, A., Pouyaud, B., Rocchia, R., Robin, E., Chaffaut, I., Moutsambote, J. M., Maziezoula, B., Censier, C., Albouy, Y., Elenga, H., Etcheber, H., Delaune, M., Sondag, F., and Gasse, F.: Origin and Function of a Closed Depression in Equatorial Humid Zones: The Lake Télé in North Congo, Journal of Hydrology, 207, 236–253, https://doi.org/10.1016/S0022-1694(98)00137-1, 1998.

Laraque, A., Bricquet, J. P., Pandi, A., and Olivry, J. C.: A review of material transport by the Congo River and its tributaries, Hydrological Processes, 23, 3216–3224, https://doi.org/10.1002/hyp.7395, 2009.

Lawson, I. T., Kelly, T. J., Aplin, P., Boom, A., Dargie, G., Draper, F. C. H., Hassan, P. N. Z. B. P., Hoyos-Santillan, J., Kaduk, J., Large, D., Murphy, W., Page, S. E., Roucoux, K. H., Sjögersten, S., Tansey, K., Waldram, M., Wedeux, B. M. M., and Wheeler, J.: Improving Estimates of Tropical Peatland Area, Carbon Storage, and Greenhouse Gas Fluxes, Wetlands Ecol Manage, 23, 327–346, https://doi.org/10.1007/s11273-014-9402-2, 2015.

Lee, H., Yuan, T., Jung, H. C., and Beighley, E.: Mapping Wetland Water Depths over the Central Congo Basin Using PALSAR ScanSAR, Envisat Altimetry, and MODIS VCF Data, Remote Sensing of Environment, 159, 70–79, https://doi.org/10.1016/j.rse.2014.11.030, 2015.

Leifeld, J. and Menichetti, L.: The Underappreciated Potential of Peatlands in Global Climate Change Mitigation Strategies, Nat Commun, 9, 1071, https://doi.org/10.1038/s41467-018-03406-6, 2018.

Limpens, J., Berendse, F., Blodau, C., Canadell, J. G., Freeman, C., Holden, J., Roulet, N., Rydin, H., and Schaepman-Strub, G.: Peatlands and the Carbon Cycle: From Local Processes to Global Implications – a Synthesis, Biogeosciences, 5, 1475–1491, https://doi.org/10.5194/bg-5-1475-2008, 2008.

Liu, H., Rezanezhad, F., and Lennartz, B.: Impact of land management on available water capacity and water storage of peatlands, Geoderma, 406, 115 521, 2022.

Loisel, J., Yu, Z., Beilman, D. W., Camill, P., Alm, J., Amesbury, M. J., Anderson, D., Andersson, S., Bochicchio, C., Barber, K., Belyea, L. R., Bunbury, J., Chambers, F. M., Charman, D. J., De Vleeschouwer, F., Fiałkiewicz-Kozieł, B., Finkelstein, S. A., Gałka, M., Garneau, M., Hammarlund, D., Hinchcliffe, W., Holmquist, J., Hughes, P., Jones, M. C., Klein, E. S., Kokfelt, U., Korhola, A., Kuhry, P., Lamarre, A., Lamentowicz, M., Large, D., Lavoie, M., MacDonald, G., Magnan, G., Mäkilä, M., Mallon, G., Mathijssen, P., Mauquoy, D., McCarroll, J., Moore, T. R., Nichols, J., O'Reilly, B., Oksanen, P., Packalen, M., Peteet, D., Richard, P. J., Robinson, S., Ronkainen, T., Rundgren, M., Sannel, A. B. K., Tarnocai, C., Thom, T., Tuittila, E.-S., Turetsky, M., Väliranta, M., van der Linden, M., van Geel, B., van Bellen, S., Vitt, D., Zhao, Y., and Zhou, W.: A Database and Synthesis of Northern Peatland Soil Properties and Holocene Carbon and Nitrogen Accumulation, The Holocene, 24, 1028–1042, https://doi.org/10.1177/0959683614538073, 2014.

Loisel, J., Gallego-Sala, A. V., Amesbury, M. J., Magnan, G., Anshari, G., Beilman, D. W., Benavides, J. C., Blewett, J., Camill, P., Charman, D. J., Chawchai, S., Hedgpeth, A., Kleinen, T., Korhola, A., Large, D., Mansilla, C. A., Müller, J., van Bellen, S., West, J. B., Yu, Z., Bubier, J. L., Garneau, M., Moore, T., Sannel, A. B. K., Page, S., Väliranta, M., Bechtold, M., Brovkin, V., Cole, L. E. S., Chanton, J. P., Christensen, T. R., Davies, M. A., De Vleeschouwer, F., Finkelstein, S. A., Frolking, S., Gałka, M., Gandois, L., Girkin, N., Harris, L. I., Heinemeyer, A., Hoyt, A. M., Jones, M. C., Joos, F., Juutinen, S., Kaiser, K., Lacourse, T., Lamentowicz, M., Larmola, T., Leifeld, J., Lohila, A., Milner, A. M., Minkkinen, K., Moss, P., Naafs, B. D. A., Nichols, J., O'Donnell, J., Payne, R., Philben, M., Piilo, S., Quillet, A., Ratnayake, A. S., Roland, T. P., Sjögersten, S., Sonnentag, O., Swindles, G. T., Swinnen, W., Talbot, J., Treat, C., Valach, A. C., and Wu, J.: Expert Assessment of Future Vulnerability of the Global Peatland Carbon Sink, Nat. Clim. Chang., 11, 70–77, https://doi.org/10.1038/s41558-020-00944-0, 2021.

https://doi.org/10.5194/egusphere-2026-5287
Preprint. Discussion started: 28 October 2026
© Author(s) 2026. CC BY 4.0 License.

Marthews, T. R., Dadson, S. J., Clark, D. B., Blyth, E. M., Hayman, G. D., Yamazaki, D., Becher, O. R. E., Martínez-de la Torre, A., Prigent, C., and Jiménez, C.: Inundation prediction in tropical wetlands from JULES-CaMa-Flood global land surface simulations, Hydrology and Earth System Sciences, 26, 3151–3175, https://doi.org/10.5194/hess-26-3151-2022, 2022.

Melton, J. R., Arora, V. K., Wisernig-Cojoc, E., Seiler, C., Fortier, M., Chan, E., and Teckentrup, L.: CLASSIC v1.0: the open-source community successor to the Canadian Land Surface Scheme (CLASS) and the Canadian Terrestrial Ecosystem Model (CTEM) – Part 1: Model framework and site-level performance, Geoscientific Model Development, 13, 2825–2850, https://doi.org/10.5194/gmd-13-2825-2020, 2020.

Menges, J., Sebag, D., Lebamba, J., Kiahtipes, C., Wotzka, H.-P., Preuß, J., Bwamangele, F. B., Lutonadio, R. K., Guardiola, M., Adatte, T., Stroobandt, Y., Bouillon, S., Garcin, Y., and Schefuß, E.: Environmental and Climatic Evolution of a River-Proximal Peatland in the Cuvette Centrale, Congo Basin, Quaternary Science Reviews, 363, 109 445, https://doi.org/10.1016/j.quascirev.2025.109445, 2025.

Mezbahuddin, M., Grant, R. F., and Hirano, T.: How Hydrology Determines Seasonal and Interannual Variations in Water Table Depth, Surface Energy Exchange, and Water Stress in a Tropical Peatland: Modeling versus Measurements, Journal of Geophysical Research: Biogeosciences, 120, 2132–2157, https://doi.org/10.1002/2015JG003005, 2015.

Nicholson, S. E.: The Rainfall and Convective Regime over Equatorial Africa, with Emphasis on the Congo Basin, in: Congo Basin Hydrology, Climate, and Biogeochemistry, chap. 3, pp. 25–48, American Geophysical Union (AGU), ISBN 978-1-119-65700-2, https://doi.org/10.1002/9781119657002.ch3, 2022.

Niu, G.-Y. and Yang, Z.-L.: Effects of Frozen Soil on Snowmelt Runoff and Soil Water Storage at a Continental Scale, Journal of Hydrometeorology, 7, 937–952, https://doi.org/10.1175/JHM538.1, 2006.

Niu, G.-Y., Yang, Z.-L., Dickinson, R. E., and Gulden, L. E.: A Simple TOPMODEL-based Runoff Parameterization (SIMTOP) for Use in Global Climate Models, Journal of Geophysical Research: Atmospheres, 110, https://doi.org/10.1029/2005JD006111, 2005.

Niu, G.-Y., Yang, Z.-L., Dickinson, R. E., Gulden, L. E., and Su, H.: Development of a Simple Groundwater Model for Use in Climate Models and Evaluation with Gravity Recovery and Climate Experiment Data, Journal of Geophysical Research: Atmospheres, 112, https://doi.org/10.1029/2006JD007522, 2007.

Niu, G.-Y., Yang, Z.-L., Mitchell, K. E., Chen, F., Ek, M. B., Barlage, M., Kumar, A., Manning, K., Niyogi, D., Rosero, E., Tewari, M., and Xia, Y.: The Community Noah Land Surface Model with Multiparameterization Options (Noah-MP): 1. Model Description and Evaluation with Local-Scale Measurements, Journal of Geophysical Research: Atmospheres, 116, https://doi.org/10.1029/2010JD015139, 2011.

Page, S. E., Rieley, J. O., Shotyk, Ø. W., and Weiss, D.: Interdependence of Peat and Vegetation in a Tropical Peat Swamp Forest, Philosophical Transactions of the Royal Society of London. Series B: Biological Sciences, 354, 1885–1897, https://doi.org/10.1098/rstb.1999.0529, 1999.

Page, S. E., Rieley, J. O., and Wüst, R.: Chapter 7 Lowland Tropical Peatlands of Southeast Asia, in: Developments in Earth Surface Processes, edited by Martini, I. P., Martínez Cortizas, A., and Chesworth, W., vol. 9 of *Peatlands*, pp. 145–172, Elsevier, https://doi.org/10.1016/S0928-2025(06)09007-9, 2006.

Page, S. E., Rieley, J. O., and Banks, C. J.: Global and Regional Importance of the Tropical Peatland Carbon Pool, Global Change Biology, 17, 798–818, https://doi.org/10.1111/j.1365-2486.2010.02279.x, 2011.

Peters-Lidard, C. D., Houser, P. R., Tian, Y., Kumar, S. V., Geiger, J., Olden, S., Lighty, L., Doty, B., Dirmeyer, P., Adams, J., Mitchell, K., Wood, E. F., and Sheffield, J.: High-performance Earth system modeling with NASA/GSFC's Land Information System, Innovations in Systems and Software Engineering, 3, 157–165, 2007.

https://doi.org/10.5194/egusphere-2026-5287
Preprint. Discussion started: 28 October 2026
© Author(s) 2026. CC BY 4.0 License.

Qiu, C., Zhu, D., Ciais, P., Guenet, B., Krinner, G., Peng, S., Aurela, M., Bernhofer, C., Brümmer, C., Bret-Harte, S., Chu, H., Chen, J., Desai, A. R., Dušek, J., Euskirchen, E. S., Fortuniak, K., Flanagan, L. B., Friborg, T., Grygoruk, M., Gogo, S., Grünwald, T., Hansen, B. U., Holl, D., Humphreys, E., Hurkuck, M., Kiely, G., Klatt, J., Kutzbach, L., Largeron, C., Laggoun-Défarge, F., Lund, M., Lafleur, P. M., Li, X., Mammarella, I., Merbold, L., Nilsson, M. B., Olejnik, J., Ottosson-Löfvenius, M., Oechel, W., Parmentier, F.-J. W., Peichl, M., Pirk, N., Peltola, O., Pawlak, W., Rasse, D., Rinne, J., Shaver, G., Schmid, H. P., Sottocornola, M., Steinbrecher, R., Sachs, T., Urbaniak, M., Zona, D., and Ziemblinska, K.: ORCHIDEE-PEAT (Revision 4596), a Model for Northern Peatland CO_2, Water, and Energy Fluxes on Daily to Annual Scales, Geoscientific Model Development, 11, 497–519, https://doi.org/10.5194/gmd-11-497-2018, 2018.

Reichle, R. H., Liu, Q., Ardizzone, J. V., Bechtold, M., Crow, W. T., De Lannoy, G. J. M., Kimball, J. S., and Koster, R. D.: Soil Moisture Active Passive (SMAP) Project Assessment Report for Version 7 of the L4_SM Data Product, NASA Technical Report Series on Global Modeling and Data Assimilation, 64, 87pp, available at: https://gmao.gsfc.nasa.gov/pubs/docs/Reichle1465.pdf, 2023.

Ribeiro, K., Pacheco, F. S., Ferreira, J. W., de Sousa-Neto, E. R., Hastie, A., Krieger Filho, G. C., Alvalá, P. C., Forti, M. C., and Ometto, J. P.: Tropical Peatlands and Their Contribution to the Global Carbon Cycle and Climate Change, Global Change Biology, 27, 489–505, https://doi.org/10.1111/gcb.15408, 2021.

Romanov, V. V.: Hydrophysics of Bogs, Israel Program for Scientific Translations, Jerusalem, 1968.

Saemian, P., Elmi, O., Stroud, M., Riggs, R., Kitambo, B. M., Papa, F., Allen, G. H., and Tourian, M. J.: Satellite Altimetry-based Extension of global-scale in situ river discharge Measurements (SAEM), Earth System Science Data, 17, 2063–2085, https://doi.org/10.5194/essd-17-2063-2025, 2025.

Samba, G., Nganga, D., and Mpounza, M.: Rainfall and Temperature Variations over Congo-Brazzaville between 1950 and 1998, Theor Appl Climatol, 91, 85–97, https://doi.org/10.1007/s00704-007-0298-0, 2008.

Scherer, D., Schwatke, C., Dettmering, D., and Seitz, F.: ICESat-2 Based River Surface Slope and Its Impact on Water Level Time Series From Satellite Altimetry, Water Resources Research, 58, e2022WR032 842, https://doi.org/10.1029/2022WR032842, 2022.

Schwatke, C., Dettmering, D., Bosch, W., and Seitz, F.: DAHITI – an innovative approach for estimating water level time series over inland waters using multi-mission satellite altimetry, Hydrology and Earth System Sciences, 19, 4345–4364, https://doi.org/10.5194/hess-19-4345-2015, 2015.

Sellers, P. J.: Canopy reflectance, photosynthesis and transpiration, International Journal of Remote Sensing, 6, 1335–1372, https://doi.org/10.1080/01431168508948283, 1985.

Shi, X., Thornton, P. E., Ricciuto, D. M., Hanson, P. J., Mao, J., Sebestyen, S. D., Griffiths, N. A., and Bisht, G.: Representing Northern Peatland Microtopography and Hydrology within the Community Land Model, Biogeosciences, 12, 6463–6477, https://doi.org/10.5194/bg-12-6463-2015, 2015.

Stocker, B. D., Spahni, R., and Joos, F.: DYPTOP: a cost-efficient TOPMODEL implementation to simulate sub-grid spatio-temporal dynamics of global wetlands and peatlands, Geoscientific Model Development, 7, 3089–3110, https://doi.org/10.5194/gmd-7-3089-2014, 2014.

Swindles, G. T., Morris, P. J., Whitney, B., Galloway, J. M., Gałka, M., Gallego-Sala, A., Macumber, A. L., Mullan, D., Smith, M. W., Amesbury, M. J., Roland, T. P., Sanei, H., Patterson, R. T., Sanderson, N., Parry, L., Charman, D. J., Lopez, O., Valderamma, E., Watson, E. J., Ivanovic, R. F., Valdes, P. J., Turner, T. E., and Lähteenoja, O.: Ecosystem State Shifts during Long-Term Development of an Amazonian Peatland, Global Change Biology, 24, 738–757, https://doi.org/10.1111/gcb.13950, 2018.

Tapley, B. D., Bettadpur, S., Ries, J. C., Thompson, P. F., and Watkins, M. M.: GRACE measurements of mass variability in the Earth system, Science, 305, 503–505, 2004.

https://doi.org/10.5194/egusphere-2026-5287
Preprint. Discussion started: 28 October 2026
© Author(s) 2026. CC BY 4.0 License.

Temmink, R. J. M., Lamers, L. P. M., Angelini, C., Bouma, T. J., Fritz, C., van de Koppel, J., Lexmond, R., Rietkerk, M., Silliman, B. R., Joosten, H., and van der Heide, T.: Recovering Wetland Biogeomorphic Feedbacks to Restore the World's Biotic Carbon Hotspots, Science, 376, eabn1479, https://doi.org/10.1126/science.abn1479, 2022.

Tian, Y., Peters-Lidard, C. D., Kumar, S. V., Geiger, J., Houser, P. R., Eastman, J. L., Dirmeyer, P., Doty, B., and Adams, J.: High-performance land surface modeling with a Linux cluster, Computers & Geosciences, 34, 1492–1504, https://doi.org/10.1016/j.cageo.2007.12.014, 2008.

Turetsky, M. R., Benscoter, B., Page, S., Rein, G., van der Werf, G. R., and Watts, A.: Global Vulnerability of Peatlands to Fire and Carbon Loss, Nature Geosci, 8, 11–14, https://doi.org/10.1038/ngeo2325, 2015.

Uhde, A., Hoyt, A. M., Hess, L., Schmullius, C., Mendoza, E., Benavides, J. C., Trumbore, S., Martín-López, J. M., Skillings-Neira, P. N., and Winton, R. S.: Mapping Peatland Distribution and Quantifying Peatland Below-Ground Carbon Stocks in Colombia's Eastern Lowlands, Journal of Geophysical Research: Biogeosciences, 130, e2024JG008 505, https://doi.org/10.1029/2024JG008505, 2025.

Waite, S.: The Global Status of Peatlands and Their Role in Carbon Cycling. A Report for Friends of the Earth by the Wetland Ecosystem Research Group, Department of Geography, University of Exeter, C.P. Immirzi and E. Maltby with R. S. Clymo (Friends of the Earth, London, 1992, ISBN 1 85750 105 5, 145 Pp., SB £17), Oryx, 27, 127–127, https://doi.org/10.1017/S0030605300020755, 1993.

Wania, R., Ross, I., and Prentice, I. C.: Integrating Peatlands and Permafrost into a Dynamic Global Vegetation Model: 1. Evaluation and Sensitivity of Physical Land Surface Processes, Global Biogeochemical Cycles, 23, https://doi.org/10.1029/2008GB003412, 2009.

Wiese, D. N., Landerer, F. W., and Watkins, M. M.: Quantifying and reducing leakage errors in the JPL RL05M GRACE mascon solution, Water Resources Research, 52, 7490–7502, https://doi.org/10.1002/2016WR019344, 2016.

Wiese, D. N., Yuan, D.-N., Boening, C., Landerer, F. W., and Watkins, M. M.: JPL GRACE and GRACE-FO Mascon Ocean, Ice, and Hydrology Equivalent Water Height CRI Filtered RL06.3Mv04, https://doi.org/10.5067/TEMSC-3JC634, ver. RL06.3Mv04, 2023.

Wösten, J. H. M., Clymans, E., Page, S. E., Rieley, J. O., and Limin, S. H.: Peat–Water Interrelationships in a Tropical Peatland Ecosystem in Southeast Asia, CATENA, 73, 212–224, https://doi.org/10.1016/j.catena.2007.07.010, 2008.

Wu, Y., Verseghy, D. L., and Melton, J. R.: Integrating Peatlands into the Coupled Canadian Land Surface Scheme (CLASS) v3.6 and the Canadian Terrestrial Ecosystem Model (CTEM) v2.0, Geoscientific Model Development, 9, 2639–2663, https://doi.org/10.5194/gmd-9-2639-2016, 2016.

Xu, J., Morris, P. J., Liu, J., and Holden, J.: PEATMAP: Refining Estimates of Global Peatland Distribution Based on a Meta-Analysis, CATENA, 160, 134–140, https://doi.org/10.1016/j.catena.2017.09.010, 2018.

Yamazaki, D., Ikeshima, D., Tawatari, R., Yamaguchi, T., O'Loughlin, F., Neal, J. C., Sampson, C. C., Kanae, S., and Bates, P. D.: A high-accuracy map of global terrain elevations, Geophysical Research Letters, 44, 5844–5853, https://doi.org/10.1002/2017GL072874, 2017.

Yamazaki, D., Ikeshima, D., Sosa, J., Bates, P. D., Allen, G. H., and Pavelsky, T. M.: MERIT Hydro: A High-Resolution Global Hydrography Map Based on Latest Topography Dataset, Water Resources Research, 55, 5053–5073, https://doi.org/10.1029/2019WR024873, 2019.

Yang, Z.-L., Niu, G.-Y., Mitchell, K. E., Chen, F., Ek, M. B., Barlage, M., Longuevergne, L., Manning, K., Niyogi, D., Tewari, M., and Xia, Y.: The Community Noah Land Surface Model with Multiparameterization Options (Noah-MP): 2. Evaluation over Global River Basins, Journal of Geophysical Research: Atmospheres, 116, https://doi.org/10.1029/2010JD015140, 2011.

Yen, Y.-C.: Effective Thermal Conductivity and Water Vapor Diffusivity of Naturally Compacted Snow, Journal of Geophysical Research, 70, 1821–1825, https://doi.org/10.1029/JZ070i008p01821, 1965.

Zeng, X. and Decker, M.: Improving the Numerical Solution of Soil Moisture–Based Richards Equation for Land Models with a Deep or Shallow Water Table, Journal of Hydrometeorology, 10, 308–319, https://doi.org/10.1175/2008JHM1011.1, 2009.